Université de Montréal

Intra- and Inter-Hemispheric Interactions in Somatosensory Processing of Pain: Dynamical Causal Modeling Analysis of fMRI data

par
Mina Khoshnejad

Département de physiologie
Faculté de médecine

Mémoire présenté à la Faculté des études supérieures et postdoctorales
en vue de l'obtention du grade de Maîtrise
en sciences neurologiques

Octobre, 2009

Université de Montréal
Faculté des études supérieures

Ce mémoire intitulé :

Intra- and Inter-Hemispheric Interactions in Somatosensory Processing of Pain: Dynamical Causal Modeling Analysis of fMRI Data

présentée par :
Mina Khoshnejad

a été évaluée par un jury composé des personnes suivantes :

Paul Cisek, président-rapporteur
Pierre Rainville, directeur de recherche
Gary Duncan, co-directeur
C. Elaine Chapman, membre du jury

Résumé

La douleur est une expérience perceptive comportant de nombreuses dimensions. Ces dimensions de douleur sont inter-reliées et recrutent des réseaux neuronaux qui traitent les informations correspondantes. L'élucidation de l'architecture fonctionnelle qui supporte les différents aspects perceptifs de l'expérience est donc une étape fondamentale pour notre compréhension du rôle fonctionnel des différentes régions de la matrice cérébrale de la douleur dans les circuits corticaux qui sous tendent l'expérience subjective de la douleur. Parmi les diverses régions du cerveau impliquées dans le traitement de l'information nociceptive, le cortex somatosensoriel primaire et secondaire (S1 et S2) sont les principales régions généralement associées au traitement de l'aspect sensori-discriminatif de la douleur. Toutefois, l'organisation fonctionnelle dans ces régions somato-sensorielles n'est pas complètement claire et relativement peu d'études ont examiné directement l'intégration de l'information entre les régions somatiques sensorielles. Ainsi, plusieurs questions demeurent concernant la relation hiérarchique entre S1 et S2, ainsi que le rôle fonctionnel des connexions inter-hémisphériques des régions somatiques sensorielles homologues. De même, le traitement en série ou en parallèle au sein du système somatosensoriel constitue un autre élément de questionnement qui nécessite un examen plus approfondi. Le but de la présente étude était de tester un certain nombre d'hypothèses sur la causalité dans les interactions fonctionnelle entre S1 et S2, alors que les sujets recevaient des chocs électriques douloureux. Nous avons mis en place une méthode de modélisation de la connectivité, qui utilise une description de causalité de la dynamique du système, afin d'étudier les interactions entre les sites d'activation définie par un ensemble de données provenant d'une étude d'imagerie fonctionnelle. Notre paradigme est constitué de 3 session expérimentales en utilisant des chocs électriques à trois différents niveaux d'intensité, soit modérément douloureux (niveau 3), soit légèrement douloureux (niveau 2), soit complètement non douloureux (niveau 1). Par conséquent, notre paradigme nous a permis

d'étudier comment l'intensité du stimulus est codé dans notre réseau d'intérêt, et comment la connectivité des différentes régions est modulée dans les conditions de stimulation différentes.

Nos résultats sont en faveur du mode sériel de traitement de l'information somatosensorielle nociceptive avec un apport prédominant de la voie thalamocorticale vers S1 controlatérale au site de stimulation. Nos résultats impliquent que l'information se propage de S1 controlatéral à travers notre réseau d'intérêt composé des cortex S1 bilatéraux et S2. Notre analyse indique que la connexion S1→S2 est renforcée par la douleur, ce qui suggère que S2 est plus élevé dans la hiérarchie du traitement de la douleur que S1, conformément aux conclusions précédentes neurophysiologiques et de magnétoencéphalographie. Enfin, notre analyse fournit des preuves de l'entrée de l'information somatosensorielle dans l'hémisphère controlatéral au côté de stimulation, avec des connexions inter-hémisphériques responsable du transfert de l'information à l'hémisphère ipsilatéral.

Mots-clés : douleur, cortex somatosensoriel, IRMf, connectivité, causalité

Abstract

Pain is a perceptual experience comprising many dimensions. These pain dimensions interrelate with each other and recruit neuronal networks that process the corresponding information. Elucidating the functional architecture that supports different perceptual aspects of the experience is thus, a fundamental step to our understanding of the functional role of different regions in the cerebral pain matrix that are involved in the cortical circuitry underlying the subjective experience of pain. Among various brain regions involved in the processing of nociceptive information, primary and secondary somatosensory cortices (S1 and S2) are the main areas generally associated with the processing of sensory-discriminative aspect of pain. However the functional organization in these somatosensory areas is not completely clear and relatively few studies have directly examined the integration of information among somatic sensory regions. Thus, several questions remain regarding the hierarchical relationship between S1 and S2, as well as the functional role of the inter-hemispheric connections of the homologous somatic sensory areas. Likewise, the question of serial or parallel processing within the somatosensory system is another questionable issue that requires further investigation. The purpose of the present study was to test a number of causal hypotheses regarding the functional interactions between S1 and S2, while subjects were receiving painful electric shocks. We implemented a connectivity modeling approach, which utilizes a causal description of system dynamics, in order to study the interactions among activation sites defined by a data set derived from a functional imaging study. Our paradigm consists of 3 experimental scans using electric shock stimuli, with the stimulus intensity changing from moderately painful (level 3), to slightly painful (level 2), and to completely non-painful (level 1) during the final scan. Therefore our paradigm allowed us to investigate how stimulus intensity is encoded within our network of interest, and how the connectivity of the different regions is modulated across the different stimulus conditions.

Our result is in favor of serial mode of somatosensory processing with thalamocortical input to S1 contralateral to stimulation site. Thus our results implicates that pain information is propogated from S1 contralateral through our network of interest comprising of bilateral S1 and S2. Our analysis indicates that S1→S2 connection is modulated by pain, which suggests that S2 is higher on the hierarchy of pain processing than S1, in accordance with previous neurophysiological and MEG findings. Lastly, our analysis provides evidence for the entrance of somatosensory information into the hemisphere contralateral to the stimulation side, with inter-hemispheric connections responsible for the transfer of information to the ipsilateral hemisphere.

Keywords : Pain, Somatosensory cortex, fMRI, Connectivity, Causality

Liste des abréviations

DCM: Dynamical Causal Modeling

fMRI: Functional Magnetic Resonance Imaging

BOLD: Blood Oxygen Level-Dependent

TR: Repetition Time

TE: Echo Time

BF: Bayes Factor

GBF: Group Bayes Factor

PER: Positive Evidence Ratio

EM: Expectation Maximization

BIC: Bayesian Information Criterion

AIC: Akaike Information Criterion

GLM: General Linear Model

ROI: Region of Interest

CC: Corpus Callosum

PCB: Posterior Callosal Body

Table des matières

Liste des tableaux

Liste des figures

Remerciements

I would like to thank my research supervisors, Dr. Pierre Rainville and Dr. Gary Duncan. I am so grateful of all their invaluable help and support. And many thanks to my family for their support and love while I was away from home.

Chapter 1- Pain Processing

Pain is a complex phenomenon and is recognized as a multidimensional experience comprising sensory, affective, motivational and cognitive components. These pain dimensions and their interactions involve spinal pathways and brain networks that transmit and process nociceptive information (1). The sensory-discriminative aspect of pain perception consists of stimulus localization, recognition of its painful nature, evaluation of its temporal features as well as quantification of its intensity. Psychophysical studies often distinguish between pain sensation and pain unpleasantness (pain affect), and these components are represented at least partly in separate regions of the brain. The affective-motivational component includes the emotional aspect of the experience, such as fear and annoyance, and it has a key role in the behavioral response to potential tissue damage. Another characteristic that subserves pain affect, aside from the immediate unpleasantness, is called the secondary pain affect and relates to emotional feelings concerning long-term implications of having pain (1). The meaning of these sensory and affective dimensions of pain is dependent upon the contextual and psychological factors, and various studies show that activation in pain areas can be highly modulated by cognitive factors like attention and previous exposure to the painful stimulus ((1) , (2)). At the cortical level, growing evidence from the physiological and imaging literature shows an extended network of pain-processing areas among which the most commonly observed sites includes primary (S1) and secondary somatosensory cortices (S2), anterior cingulate cortex (ACC), as well as insula, frontal and prefrontal cortices (3). It is a widely held idea that S1 and S2 contribute to the sensory aspects of nociceptive processing, however the relative contribution of each and their functional organization have been in dispute. In this chapter, Section 1-1 presents a brief review of the literature on the main ascending pathway of the nociceptive system from the spinal cord to the various cortical areas that receive and process noxious information; section 1-2 reviews supporting evidence from clinical, neurophysiological and imaging studies for the involvement of S1 and S2 in pain perception. Section 1-3 consists of a short discussion on the functional organization and interactions between S1 and S2 and

a short review of the assumption in our hypothesis, which is discussed in detail in section 1-4 and section 1-5.

Section 1-1: Afferent Pain Pathways

Propagation of pain is initiated with a peripheral stimulus (mechanical, electrical, thermal, or chemical) activating specific receptors called nociceptors, which are widely found in the skin, visceral organs, and muscles. These first-order afferent fibers consist of small-diameter thinly mylinated A-Delta or unmylinated C fibers that have their cell bodies within the dorsal root ganglia and their axon terminals in the dorsal horn of the spinal cord. These first-order neurons form synapses with second-order neurons distributed within the dorsal horn of the spinal cord. The second-order neurons in the dorsal horn are classified into 3 distinct categories, and the organization of the ascending pathways depends upon them (4).

Group 1- Nociceptive Specific (NS) neurons respond exclusively to noxious stimuli and are located in superficial layers of the dorsal horn, especially in lamina I. They receive inputs from A-Delta and C fibers, and their receptive fields show somatotopic organization mostly in Lamina I (4).

Group 2- Wide Dynamic Range (WDR) neurons respond to both noxious and innocuous stimuli and are located in deep dorsal horn (Laminae IV-V) (4). They are activated by A-Delta, A-Beta, and C fibers and code for stimulus intensity across the entire range of sensation.

Group 3- Non-Nociceptive neurons (NN) respond to innocuous stimuli and are activated by A-Delta, and A-Beta fibers.

The axons of the second-order neurons decussate and form afferent bundles that ascend through the anterolateral and dorsolateral funiculus, relaying nociceptive

information to structures of the brain stem (reticular formation of medulla, PAG, etc) and thalamus. This pathway, called the spinothalamic tract (STT), is one of the principal ascending tracts of the spinal cord. The dorsolateral STT carries information mainly from Lamina I of the dorsal horn (as well as V-VI (1)) and terminates in the medial nuclei of thalamus, whereas axons from anterolateral STT originate from deep layers of the dorsal horn and project to lateral nuclei of thalamus (5). The terminations of the spinothalamic tracts in different thalamic nuclei (and the cortical projections from these nuclei to the cortex) form different circuits for pain processing. The projections to cortex from cells in medial and lateral thalamic nuclei are known as the medial and lateral pain systems, respectively, which operate in a parallel manner.

The lateral system which is believed to be primarily involved in the sensory discriminative aspect of pain processing, includes the lateral nuclear complex of thalamus, consisting of ventropostero-lateral (VPL), ventropostero-medial (VPM) and ventropostero-inferior (VPI) nuclei that project collectively to S1 and S2 cortex (4). VPL and VPM mainly consist of WDR type neurons, while NS neurons predominate in VPI nuclei. Animal studies have shown that VPI projects to S2 cortex while VPL projects to S1 cortex (5). These neurophysiological data show that stimulus characteristics are evaluated in the lateral system by WDR neurons of S1, which encode for the intensity of the stimulus, and by NS neurons of S1, which code for the spatial and temporal properties of the stimulus. Nociceptive neurons in S2 have been reported to mainly code for the temporal structure of the stimulus (4).

The medial nociceptive system consists of projections from medial thalamic nuclei to limbic structures like the insula and the anterior cingulate cortex. The cingulate cortex has been implicated in the attribution of emotional significance to the painful stimulus, in the regulation of emotional responses to noxious stimuli, and in the integration of cognitive, affective, and attentional responses (4). In brief, the medial pain system relates to affective-motivational dimensions of pain perception and is involved in processing cognitive,

behavioral and autonomic reactions to noxious stimulation. Apart from the specific research articles cited above, the reader may consult a general review of this literature by Kandel et al (6) for additional information.

Section 1-2: Involvement of Primary and Secondary Somatosensory areas in pain perception

Somatosensory areas S1 and S2 are the two principal cortical areas that are thought to be implicated in the processing of both noxious and innocuous tactile stimuli. S1 in monkeys consists of 4 separate cytoarchitectonically defined areas; areas 3a, 3b, 1 and 2, with a somatotopic representation of the contralateral body surface in each architectonic field (6). S2 is located in parietal operculum in the upper bank of Sylvain fissure just inferior and lateral to S1. Converging lines of evidence from clinical and experimental studies indicate that S1 and S2 are involved in nociception and especially in sensory-discriminative aspects of pain perception; this evidence is discussed below.

Neurophysiological evidence from non-human primates shows that neurons in S1 receive input evoked by noxious stimuli. These nociceptive neurons encode for stimulus intensity by their firing rates (7), and their peak discharge frequency is significantly correlated with the monkey's speed for detecting increases in the noxious level of thermal stimulation (7). The intensity-encoding property has also been observed for WDR neurons of VPL that project to S1 (8). Various studies demonstrated a detailed somatotopic organization within S1, which implicates the role of this region in encoding the spatial localization of the pain stimulus. Localization is important for sensory processing as well as for the quick orientation of attention to, and withdrawal of the body part from, the source of nociceptive stimulation – processes needed to prevent or limit potential tissue damage.

In contrast to S1, animal studies show that only small populations of S2 neurons are responsive to noxious stimuli, while the majority of neurons in S2 respond to innocuous

somatic stimuli. Some evidence from animal and human studies suggests separate representations of pain and touch in the parietal operculum (9). It has been demonstrated in primates that S2 nociceptive neurons have large receptive fields and are not capable of a precise encoding of stimulus intensity. They are responsive to bilateral as well as contralateral stimulation of the body and receive their inputs from NS neurons of VPI, which show the same response characteristics. It has been argued that because S2 projects to limbic areas via the insula, it might have a role in pain learning and memory (5). It has been discussed by Schnitzler (5) that, for the tactile system S2 is involved in feature extraction such as roughness discrimination (6) and detection of object size. Also lesion studies show that ablation of the S2 region impairs recognition of object shape (10). Additionally evidence suggesting that S1 and S2 are reciprocally connected to each other ((11), (12)) implies a functional interdependence between the two in pain processing. However, the role of S1-S2 interactions in pain has not yet been explored specifically.

Aside from neurophysiological studies, multiple case reports in clinical and lesion studies demonstrate an essential role of S1 and particularly S2 in normal pain perception. Potagas et al (13) reported a case of a woman who had episodic pain in the right side of her body, which was associated with a lesion in the white matter of the parietal operculum. Pain disappeared, after the surgical removal of the tumor. Greenspan et al (14), report a patient whose impairments in both pain and tactile perceptions (higher mechanical and heat thresholds and poor ability to discriminate roughness on the hand) were associated with a tumor located near the posterior insula and parietal operculum contralateral to the perceptual deficits. After surgery, the patient's somatic deficits disappeared, which again suggest the essential role of S2 in the normal experience of pain and tactile perception. Ploner et al (15) report a case of a patient who described an unpleasant feeling following noxious stimulation but could neither localize the stimulus nor recognize its noxious nature; association of these symptoms with an ischemic lesion that included S1 and S2 implicates these areas in sensory-discriminative processing of noxious information and suggests that affective pain processing, which remained at least partly intact, likely involves regions

outside the somatosensory cortices. In a recent study by Greenspan et al (16), 6 patients with lesions in the parasylvain cortex (parietal operculum, and posterior insula) were tested for their pain sensitivity. Their results show that the 4 patients with lesions involving the posterior parietal operculum showed elevated thresholds for mechanical- and heat-evoked pain on the contralateral side, whereas the 2 subjects with lesions in posterior insula showed no pain threshold alterations. However these 2 patients exhibited deficits in motivational and affective response to pain (as indicated by a cold pain tolerance test), which suggests a role of posterior insula in pain affect. Another observation in this line of investigation is an experiment by Dong et al (17), involving awake monkeys, which showed that damage induced in the left posterior parietal cortex changes the monkey's pain sensibility on the contralateral face. Thus, lesion studies generally provide at least some support for a role of parietal cortices, including S1 and S2, in pain processes.

Some studies have proposed that nociceptive input into S1 may have more to do with modulation of tactile sensation. The information that is being conveyed by the different somatosensory sub-modalities of touch, thermal sensation and pain interrelate with each other to some extent. The influence of touch on pain perception has been addressed in 1965 by Melzac and Wall in their "Gate Control Theory of Pain", which asserts that the fibers conveying innocuous touch information can interfere with nociceptive signals and therefore inhibit pain perception. Apkarian et al (18) described the opposite interaction, the effect of pain on touch perception, which they called the "Touch Gate", arguing that the presence of heat-induced pain can significantly diminish tactile sensation. In their study, they compared the simultaneous presentation of noxious heat and vibrotactile stimulus on the right hand with the presentation of the vibrotactile stimulus alone, measuring the vibrotactile thresholds before, during and after application of the painful heat. The results show increased vibratory thresholds and decreased tactile sensitivity, during and after painful thermal stimulation. Increases in vibratory thresholds occurred around subject's pain thresholds, which indicated that activation of nociceptors indeed diminish the encoding of vibrotactile inputs. It has been argued that this effect might be

cognitive in nature, that attentional mechanisms might interfere with the perception of tactile sensation; however, this can be possibly ruled out by the observation that the tactile and painful stimulus must be within the same ipsilateral sites for the heat-induced pain to inhibit vibrotactile sensation (19).

Imaging studies generally report significant increases of cereberal blood flow (CBF) in the parietal operculum associated with painful stimulation. But early imaging studies reported inconsistent results on the role of S1 in pain perception. In a PET study by Talbot et al (20), a noxious heat stimulus applied sequentially to 6 spots on the forearm was associated with significant activation in the contralateral S1, presumably in response to the evoked pain. In a similar experiment by Jones et al (21), a heat stimulus presented to a single spot on the dorsal hand failed to produce significant activation in S1. In a subsequent PET study by Apkarian et al (22), putting the subject's fingers in hot water led to decreased activity in S1. More recently, Timmerman et al (23) used fMRI to demonstrate a high correlation between S1 activity and both the intensity of noxious stimulation and the pain ratings evoked by that noxious stimulation; these results are in line with many of the more recent studies, which further support the involvement of S1 for intensity encoding of noxious stimuli.

Various arguments have been proposed by Bushnell and colleagues (2) to explain inconsistencies in the early imaging studies, most notably the uncontrolled but significant modulation of S1 activity by cognitive factors like attention and suggestions. They note that when attention is directed away from a painful stimulus, the activity in S1 is significantly reduced. Carrier et al (24)scanned subjects while they performed psychophysical tasks in which they had to attend to, and detect, small changes in either the noxious thermal intensity or the auditory tonal frequency of simultaneously presented stimuli. Pain intensity was rated lower and SI activity was reduced during the auditory, compared to the thermal, task. In studies from the same research group, Hofbauer et al ((25),(26)) observed that changes in the perceived intensity of pain, produced through hypnotic suggestions (a

cognitive manipulation), are directly correlated with activity in S1; however, suggestion-induced changes in pain unpleasantness, performed in a second hypnosis experiment by Rainville et al (27), were correlated with activity in ACC, but not in the activity of S1. Altogether these results suggest that the activation in S1 is highly dependent on cognitive factors like attention or suggestion, and changes in S1 activity are associated with changes in the subject's perception of pain intensity.

If S1 and S2 are indeed involved in pain and tactile perception, the time course of pain-evoked and tactile-evoked activity in the somatosensory cortices should reflect the ongoing perception of those stimuli. Chen et al (28), tested this hypothesis in an experiment consisted of the presentation of noxious heat and innocuous brush stimuli of the same duration (9 sec). Analyses of the time course of activation in S1 and S2, revealed remarkable differences in the temporal domain with tactile-related activity peaks immediately upon stimulation and then habituates whereas the pain evoked activity has a slower onset, and keeps rising towards an eventual peak that occurs 8 sec after the stimulus offset. Thus the study confirms the hypothesis that activity in S1, evoked by noxious stimuli, is temporally correlated with the continuing perception of pain that follows stimulus offset, whereas tactile perception occurs around the stimulus offset.

Altogether the experimental data from neurophysiological studies, clinical observations of brain lesions, and evidence from the brain imaging literature, implies an important role of the somatosensory cortices in the experience of pain. This evidence for a contribution of both S1 and S2 in pain, motivated us to study the interactions between these areas in the processing of noxious information. Our hypothesis and the assumption underlying it, is discussed in the following section.

Section 1-3: Hierarchical organization of S1 and S2

Anatomical studies show that S1 is linked with S2 via intracortical reciprocal connections ((11), (12)). Pain and tactile information may therefore be conveyed to S2 through an indirect or serial path from the thalamus via S1. However as discussed in the previous sections, various studies of non-human primates suggest that S1 and S2 both receive direct projections from the thalamus, and it is likely that they are hierarchically organized in a parallel thalamocortical processing network. But as discussed in the previous section there are segregated nociceptive pathways from the spinal cord to S1 and S2, and the different thalamic nuclei that project to S1 and S2 have different response characteristics. Therefore they convey different information to S1 and S2. Since the response characteristics of nociceptive neurons of S1 and S2 are quite different, it is possible that input to S1 would be sufficient for the processing of one aspect of pain (ex; sensory discriminative aspect). Though if the stimulation paradigm triggers dimensions of pain other than intensity encoding, then the parallel thalamocortical input to S2 may perhaps be essential for the perception of pain that results from the interactions of various dimensions. This is one of the ideas that we wanted to address in this study through causal modeling of regional interactions.

Thus, functional organization in the somatosensory cortex is a matter of dispute, and relatively few studies directly examined integration of information between somatic sensory regions; this includes the hierarchical relationship between S1 and S2, as well as inter-hemispheric connections of the homologous somatic sensory areas. The purpose of this study was to test some causal hypotheses on the interactions between S1 and S2, while subjects were receiving painful electric shocks. We systematically tested a set of models of integration between S1 and S2 including intra-and inter-hemispheric connections in the context of pain.

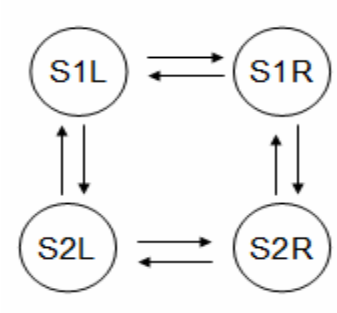

Figure 1-1. Intrinsic connection between S1 and S2

Based on the organization of the cortical somatosensory system, we postulated intrinsic connections among these sensory areas as shown in Figure 1-1. Then we tested a set of hypotheses based on: 1) which connections in this intrinsic network are modulated by the painful stimulus and 2) where the direct effect of noxious stimulus is most likely to occur and thus cause a change in the activity of the somatosensory regions by propagating its effect throughout the network. The complete description of the operational hypotheses is provided in chapter 2. As depicted in Figure 1-1, we assumed intra-cortical connections between S1 and S2 in both hemispheres as well as inter-hemispheric connections between homologous areas of S1 and S2. This section provides background from anatomical, neurophysiological, imaging, MEG and sensory evoked potential studies in support of such assumptions. The rest of this section is organized into sub-section 1-3-1 (describing intra-hemispheric connections) and sub-section 1-3-2 (which describes the inter-hemispheric connections).

Section 1-3-1: Intra-hemispheric connections between S1 and S2

1-3-1-1: Increase in the complexity of Receptive Fields

The notion of sequential sensory processing implies the processing of gradually more complex sensory features of the stimulus in a hierarchical order of cortical areas. This

implies neurons with more complex receptive field characteristics in the hierarchy of processing flow.

Various single-cell recording studies in the somatosensory cortex have confirmed that there is a systematic increase in the complexity of neuronal receptive field's (RF) properties along the rostro-caudal axis of the post-central gyrus ((29), (30)). Iwamura et al (31) observed that the complexity of RF of the hand region increases from area 3b to area 1 and 2 and towards the upper bank of intraparietal sulcus. Likewise, Duffy and Burchfiel (32) demonstrated in extracellular recordings from area 5 of monkeys, performed while manipulating multiple joints of one or more limbs, that the RF of cells in area 5 are sensitive to multi-joint limb manipulation, while neurons in the lower order processing regions only show sensitivity to single-joint manipulations. The number of bilateral RF neurons also increases towards the caudal part of the post central gyrus (33).

Also various studies had shown that the RF properties of bilateral neurons in S2 are even more complex than S1 ((34), (33)). In a study by Fitzgerald et al (35), it has been demonstrated that most S2 hand-region neurons have multidigit RFs, suggesting that S2 is of a higher order than area 3b (which primarily has single-digit RFs) and therefore that S2 has a role in integrating information across separate digits.

All together these data imply a sequential mode for sensory processing, with S2 at a higher order of the hierarchy for the processing of more complex details of stimulus features. However this notion has not been tested in the pain system, and although earlier studies show nociceptive neurons in S1 and S2, they did not test for a possible increase in the complexity of nociceptive neurons across these areas.

1-3-1-2: Ablation studies

Anatomical studies in monkeys ((11), (12)) reveal that architectonic fields in S1 are interconnected and that S1 and S2 are connected to each other in a reciprocal organized

manner. The question of whether tactile or noxious input to S2 comes via an anatomical pathway from S1 or from direct projections from thalamus can be tested through inactivation of S1 or S2 by surgical ablation methods or reversible cooling procedures; specifically, one can test whether inactivation of S1 affects S2 responsiveness or vice versa. Localized cooling provides a method for selective and reversible block of synaptic transmission within particular regions of the cerebral cortex (36). A summary of such ablation studies using both methods is discussed below.

Various cooling-induced ablation experiments on cats provide evidence for a parallel processing scheme. In anesthetized cats, Turman et al (37), investigated whether the inactivation of the distal forelimb region within S1 effect S2 responsiveness. The results indicate 20% of S2 neurons showed a reduction in their activation level, but that the majority of S2 neurons (80%) revealed no change at all in their response level. Although the observed reduction in the minority of the population can be attributed to the removal of facilitatory influences exerted via the intra-cortical connections between S1 and S2, the majority survived the inactivation, which implies a parallel mode of processing as the main mechanism. The reverse procedure was employed in another study by Turman et al (38), who examined the responsiveness of neurons in the distal forelimb region of S1 after the inactivation of the corresponding region of S2 through a cooling-induced procedure. Approximately 60% of S1 neurons were unaffected by S2 inactivation but the remaining 40% displayed some reduction in their response level. A similar study by Murray et al (36), in rabbits tested the effect of S1 inactivation on the neuronal activity in S2 (within the distal forelimb and hindlimb region) evoked in response to tactile stimulation. The vast majority (93%) of S2 neurons were unaffected by S1 inactivation, while only 7% showed a reduction in their response level. Thus, the ablation studies conducted in lower mammals, like cats and rabbits, provide similar results in favour of parallel processing of somatosensory information.

In contrast, studies in monkeys provide evidence for a serial processing scheme. Garaghaty et al (39) partially ablated the hand representation in area 3a and 3b of marmoset monkeys, and then recorded from S2 regions after the lesion. Their results showed that the somatotopically corresponding areas in S2 were no longer responsive to cutaneous stimulation of hand but other areas of S2, representing other body parts, remained responsive to tactile stimulation. In a similar study, Burton et al (40) ablated the hand representation in primary somatosensory cortex (S1) of Macaca monkeys and recorded in ipsilateral second somatosensory cortex (S2) a year later. They found that significant portions of the S2 hand area were unresponsive to cutaneous stimulation of the hand, which suggests that S2 responses depend heavily on inputs from S1 for its activation even after such a long period following S1 ablation.

As discussed in section 1-2, S1 comprises of 4 cytoarchitectonic subdivisions; areas 3a, 3b, 1, and 2, with each area responsible for processing different components of somatosensory information. Areas 3b and 1 process mainly cutaneous inputs, whereas the other two process information from afferents coming from “deep” body tissues such as muscle (area 3a) and joints (area 2) (6). Pons et al (41) investigated the relative influence of each of these S1 areas on the responsiveness of neurons in the hand representation in S2 of macaques, using ablations of the hand representations in areas 3a, 3b, 1, and 2 in different combinations. Their results show that ablation of areas 3b and 1 resulted in S2 responsivity to only deep stimulation because only deep input were provided for S2, whereas ablation of 3a and 2 yeilded strong S2 responses only to cutaneous inputs as the result of the absence of deep inputs. Combined ablation of cortical areas 1 and 2 only altered the ratio of cutaneous to deep receptive fields, but S2 neurons were still responsive to both cutaneous and deep input because area 3a and 3b relay the corresponding information to S2 hand region. The same was true for the combined ablation of 3a and 3b. It is interesting to reflect that other than the hand representation in S2, other areas remained intact in their responsivity to either cutaneous or deep stimulation.

Since several studies showed that in simian primates S2 responsiveness was abolished by surgical ablation of S1 and that S1 responses were significantly diminished following S2 lesions, these results seem to be in favour of hierarchical processing of somatosensory information in the parietal cortex. However results from studies in cats and rabbits are more in favour of parallel processing, suggesting that there may be fundamental differences between simian primates and other mammalian species in the organization of thalamo-cortical systems. It has been hypothesized by Pons et al (41) that there might have been an evolutionary shift from parallel processing in general mammals to serial organization in higher primates. In humans, evoked potential studies provide further information on this issue as discussed in the following subsection.

1-3-1-3: Evoked Potential Studies

If the flow of somatosensory processing is serially organized, cortical responses in S1 and S2 should perhaps show considerable differences in their response latency to somatic stimulation. Various studies have used magnetoencephalography (MEG) or electroencephalography (EEG) to record sensory evoked potentials in an attempt to elucidate temporal relationships among the various cortical areas in the post-central gyrus in response to noxious and innocuous stimulation. These methods allow the localization of cortical sources as well as measurement of the time taken for the signal transfer in the brain.

Although some MEG studies show simultaneous activation of S1 and S2 (implicating a parallel mode of sensory information processing in S1 and S2), other studies contradict this idea. The reason for this controversy across studies may reflect the weak activation magnitude of S1 and thus the difficulty to find early S1 activity (42). It has been further argued by Inui et al (42) that the weakness of S1 activity might be explained by the weaker stimulus intensity of noxious stimulation used in some studies. Since the level of activity of S1 nociceptive neurons has been shown to encode stimulus intensity, activation

by low intensity stimuli may be more difficult to detect with this method. In contrast, since S2 neurons may play roles other than intensity encoding, S2 responses may be easier to detect at lower stimulus intensity.

Activation latencies of the various somatosensory areas following application of transcutaneous non-painful electrical stimulation has also been studied using MEG by Inui et al (30). The results show a significant shift of onset latency from area 3b to areas 1, 5 and S2 respectively. Although these results may imply a sequential mode of processing, one possible alternative explanation is that all these activations come directly from the thalamus and the observed response latency can be attributable to the different conduction velocities from the thalamus (as discussed by Inui et al in (30)). However, it has been shown in animals by Salami et al (43) that the latencies of thalamocortical afferents that convey information from the thalamus to multiple cortical areas are almost the same, irrespective of the distance.

MEG recordings following application of painful and non-painful electrical stimulation to the hand have been analyzed to identify the source location and activation latencies within S1 and S2. Using this technique, Inui et al (42) found that the source locations for activation sites evoked by noxious and innocuous stimulation were relatively similar in S1 and S2, except that innocuous stimulation activated 2 sources in S1. Those 2 sources in S1 had a short latency (<40 msec) and originated in area 3b and in area 1. Early activity following noxious stimulation was localized only in area 1, and in this case, the latency was longer than 85 msec (longer latencies for pain-evoked cortical activation are explained by the slower conduction velocities of peripheral nociceptive afferents, rather than differences in cortical interconnections). S2 activation always followed S1 activity. Relative to S1 peaks, the onset latency of S2 responses were delayed by 29 ms and 35 ms following noxious and innocuous stimulation, respectively. Because of the significant difference in onset latency between S1 and S2, these results strongly favor serial processing for both nociceptive and tactile information. The response delays from S1 to S2 were

almost the same between innocuous (35 ms) and noxious stimulation (29 ms), which suggests that information from S1 to S2 is being transmitted through similar pathways, consistent with the dynamics of cortico-cortical connections.

In another study by Kitamura et al (44), which focused on cortical responses to noxious stimulation, MEG was used to record somatosensory evoked magnetic fields (SEF) associated with 'weak' and 'strong' painful transcutaneous electrical stimulation delivered to the left sural nerve at the ankle. Early deflections (< 100 ms in latency) were located in S1 contralateral to the stimulated nerve, which was identified in both weak and strong stimulation sessions. A middle latency component (> than 100 ms) was also found in bilateral S2 and cingulate cortex – but only in the strong stimulation condition (two sources were described, one with a latency of 150 msec and the second with a latency of 250 msec). Following in this line of study, Kakigi et al (45) investigated SEF after stimulation applied to various body parts in five normal subjects. In agreement with the results from lower limb stimulation (44), stimulation of the right and left posterior tibial nerves at the ankle in all subjects resulted in early activation in the foot area of S1. Small middle-latency deflections were clearly identified in two subjects in the second somatosensory cortex (S2) in both hemispheres with 100 ms latency. The same temporal order of activation was also found following upper limb stimulation of the median nerve at the wrist or fingers. In conclusion, all these studies indicate that, following a painful stimulation, S1 is initially activated, and then S2 is activated with a delay of 30-50 msec, depending on the stimulation site.

In brief, section 1-3-1 addressed the issue of intra-hemispheric connections of S1 and S2. Section 1-3-1-1, discussed the increase in the complexity of neuronal RFs from S1 to S2, consistent with the notion that S2 is a higher order processing unit. In section 1-3-1-2, some ablation studies have been reviewed, which show that in higher order primates normal S1 and S2 activity is dependent upon their reciprocal interactions. And lastly the evoked potential studies described in subsection 1-3-1-3 showed that S2 is activated later than S1, which suggests that the dominant flow of information is from S1 to S2, in favour

of a serial processing scheme. In what follows (section 1-3-2), the inter-hemispheric connections in the somatosensory cortex are discussed.

Section 1-3-2: Inter-hemispheric callosal connections

1-3-2-1: Anatomical studies

The Corpus Callosum (CC) is the main fiber tract that mediates communication between homotopic regions of somatosensory cortex. Anatomical investigations reveal that the macaque's homologues of human S1 and S2 have dense callosal connections ((46),(47)) .These early studies found that the distribution of callosal fibers is not uniform, with midline structures of body representation (head, trunk, tail and proximal limb regions) having dense callosal connection and the distal limb regions having fewer commissural fibers (46). As discussed in previous sections, S1 contains multiple somatotopic representations of the body surface, which are defined by individual architectonic fields, and these early studies also report that even within the connected zones, the density of callosal connections varies, with increasing density across areas 3b, 1 and 2 (46). Likewise, even within each architectonic field, the representations of hand and foot have fewer callosal connections than face and trunk (46).

Recent studies, perhaps with the benefit of more sensitive anatomical techniques, describe callosal connections for peripheral body parts, in addition to those for midline structures, which were emphasized in the initial reports. In a study by Iwamura et al (31), a large number of neurons with bilateral RF have been found in the digit regions within the upper bank of the intraparietal sulcus. The RF of these neurons show very complex characteristic compare to neurons in the anterior part of post central gyrus that projects to them (31), which implicates the hierarchical processing of somatosensory information. These bilateral neurons could not be found after lesioning the postcentral gyrus in the opposite hemisphere. This suggests that bilaterality is the result of a transfer of

somatosensory signals from the contralateral hemisphere via callosal connections. In a more recent study, Iwamura and colleagues ((33),(48)) describe a significant number of neurons with bilateral RFs in the hand, digits and lower extremity areas within the caudal part of post central gyrus in the awake monkey. Likewise, Taoka et al (49) found bilateral RFs in the hindlimb region of postcentral somatosensory cortex mostly in areas 2 and 5. The ipsilateral input for these bilateral receptive fields possibly reaches the cortex via callosal fibers from the contralateral site. Iwamura et al (48) also demonstrate that callosal connections are more dense and bilateral activity becomes more widespread and complex in S2 and in the caudal parietal areas. This finding again supports the notion that these areas are involved in higher-order stages of processing of somatosensory information.

In general, data from experiments on non-human primates ((46),(47)) strongly support the hypothesis that callosal connections are responsible for sensory activation of ipsilateral cortical sites after sensory afferent activity is relayed from the homologous somatic sensory area. In human subjects, latency studies have shown that ipsilateral activation that is elicited by tactile stimulation is delayed relative to the homototopic contralateral activation by a time lag corresponding to the interhemispheric transmission time (50). Therefore it is quite probable that anatomical and functional organization of the human and non-human primate somatosensory cortices would be similar.

1-3-2-3: Studies on Callosotomized and Acallosal patients

The idea that peripheral sensory information from ipsilateral body sites reaches the ipsilateral hemisphere through commissural fibers of the corpus callosum can be investigated by studying the callosotomized patients (surgical section of some part or all of the corpus callosum) and acallosal individuals (individuals born without corpus callosum). Studying the patterns of cortical activation by imaging modalities as well as examining the performance of these patients in tasks that require interhemispheric integration of sensory inputs allows testing the contribution of the CC to this function.

Fabri et al (51) described a fMRI study in which 6 healthy and 3 callosotomized patients (complete callosotomy) were tested for their cortical responses to tactile and mechanical painful stimulation (pricking the palm with a sharp probe). The results show contralateral S1 and bilateral S2 activation in response to noxious stimuli in both patients and normal controls. The ipsilateral S2 response in the patients may implicate ipsilateral pathways or extra-callosal fibers conveying nociceptive information across hemispheres. The tactile condition only evoked contralateral activation in S1 and S2 in the patients but bilateral activation in S2 and contralateral S1 in the control group. This demonstrates that the inter-hemispheric transfer of non-nociceptive information depends more heavily on the integrity of the CC.

In another study Fabri et al (50) reported an fMRI experiment conducted on 12 callosotomized and 12 control subjects. Subjects received unilateral tactile stimulation, which consisted of brushing the subject's palm and finger with a rough sponge. Three callosotomized subjects had a total resection of CC and nine had a partial resection only. Consistent with their late study, discussed above, results showed that unilateral tactile stimulation provoked contralateral activation in S1 and bilateral activation in S2 cortices in normal subjects. In the 3 split-brain patients and 7 of the partial callosotomy subgroup, there was a complete absence of S1 and S2 activation in the ipsilateral hemisphere, but contralateral activation was similar to those obtained in normal subjects. Activation in S2 of the ipsilateral hemisphere was observed only in two patients with intact splenium and posterior body of the CC.

In a very recent study, Duquette et al. (52) tested two acallosal, one callosotomized, and six healthy control subjects in an fMRI study investigating cortical responses to both tactile and painful stimulation. Their paradigm consisted of 3 experimental runs of tactile stimulation (brushing of the subject's calf) and 3 runs of thermal stimulation (noxious heat and innocuous warm stimuli). Bilateral tactile activation was found in S1 and S2 in some control and acallosal subjects but ipsilateral activation was not observed in the

callosotomized subject. This result suggests a reorganization of the touch system in acallosal subjects and the existence of compensatory mechanisms that may be responsible for the bilateral activation in these patients with a compromised CC. But consistent with previous reports, in the pain condition, all subjects including the callosotomized patient showed bilateral activation in at least 2 pain areas (S2, ACC, and/or in Insula). Bilateral activation in the callosotomized patient may indicate the potential independence of the pain system from callosal connections; however, since the study only included one callosotomized patient, their result cannot be generalized to normal subjects, as this could also reflect plasticity in the callosotomized patient.

Fabri et al (53) recently investigated the relative contributions of different portions of CC for the transfer of tactile information. Anatomical studies on non-human primates had previously indicated that the CC is topographically organized with anterior fibers connecting the frontal lobes and the posterior fibers connecting temporal, parietal and occipital lobes (54). Consequently patients with a lesion at different locations of the CC should show deficits reflecting this organization. Consistently, Fabri et al (53) reported that callosotomized patients with resection in the posterior part of CC show tactile-evoked activations only in the contralateral hemisphere while patients with an intact posterior callosal body (PCB) show bilateral tactile-related activation like normal subjects. Aside from the imaging results, their neuropsychological data are also interesting. The “Tactile Naming Test” evaluates the participant’s ability to name tactile stimuli that are presented only to the left hand – i.e. evaluates the ability of tactile-related processing to transfer from the hemisphere contralateral to stimulation to the opposite hemisphere where it can be accessed by left-lateralized language areas. The results show that only the patients with intact PBC performed well, obtaining high scores in this test. This provides support for the notion that the interhemispheric fibers running through the posterior portion of CC are necessary to convey tactual information to the left hemisphere where its description can be verbalized

In section 1-3-2, we have provided a brief overview of the inter-hemispheric communication between homologous somatosensory cortices. Section 1-3-2-1 discussed some of the anatomical studies in support of callosal connections, and Section 1-3-2-2, reviewed imaging studies on callosotomized and acallosal patients. In brief these studies show the absolute absence of tactile-related activation or partial lack of pain-related activation in the ipsilateral S1 and S2 for callosotomized, while for normal subjects bilateral S2 activation has been observed. These results emphasize the role of CC for conveying the noxious and innocuous information to the ipsilateral regions. However, since in the pain condition, ipisilateral activation has been observed in some regions within the pain matrix in callosotomized patients, one other possibility would be that thalamocortical projections directly relay nociceptive input to the ipsilateral sites in these patients. But this possibility must be treated with caution, since it is based on very limited lesion data, therefore more conclusive evidence awaits additional studies of callosotomized patients and a more detailed analysis of neuronal networks of nociceptive processing. Causal modeling which we implemented in this study to investigate the nociceptive processing within the somatosensory cortex in normal subjects, tries to address the question of callosal transfer of information from a causal perspective. The mathematical detail of this modeling is discussed in the next chapter.

Chapter 2- Dynamic Causal Modeling

Section 2-1: Introduction

Usually the main focus of neuroimaging studies is functional localization, in which a particular brain region is associated with a specific function. However this definition of functional localization is incomplete, since a cortical area does not work in isolation but is related to a particular cortical circuitry involved in achieving a specific sensory, perceptual, affective, cognitive or executive function. Recent approaches to functional integration model interactions among various specialized areas in order to study functional architecture.

The numerous approaches that have been developed to study functional integration can be categorized into two main groups: functional connectivity and effective connectivity. The approaches grouped under the term functional connectivity attempt to explain the activity in one area in relation to activity elsewhere by looking at correlations between the two. However a correlation between the two regions does not necessarily constitute direct evidence for integration between the two, since the correlation might be due to the involvement of a third structure which feeds into the two regions of interest, thus causing the correlation between them.

The other group of approaches to the study of functional integration, effective connectivity, is focused on the causal influence that one neuronal population applies over the other. Integration among various regions is usually better explained and defined conceptually in terms of effective connectivity. The approach being described and used here; “Dynamical Causal Modelling” (DCM) belongs to this class of modelling. DCM is a method proposed by Friston et al (55) to test causal hypotheses about integration among specialized brain regions using functional imaging data. DCM models interactions among neuronal populations at a regional cortical level using fMRI time series. The aim of this kind of modeling is to estimate the parameters associated with the strength of the connections among brain regions and to examine how that coupling is influenced by

changes in an experimental context (56). In general, by using DCM, one can hypothesize which pathway has been activated by experimental manipulation, as opposed to a cortical region that might be identified using a conventional General Linear Model (GLM) analysis (56).

The following Section 2-2, provides a general introduction to system theory. Section 2-3 contains a complete description of the methodology together with a discussion of the assumptions and limitations of DCM. Section 2-4 describes the Bayesian scheme for the estimation of model parameters. The chapter finishes with a discussion of the different criteria used for model selection (Section 2-5).

Section 2-2: A general introduction to System theory

The dynamics of the brain and the interactions among its various regions can be framed from a "System" Perspective. In general, a system is a set of elements that interact with each other in a temporal manner (57). Assume a system that has n elements with a time-varient property x_i associated with each element. Each of these constituent elements $x_i\ (1 < i < n)$ is called a state variable. The state vector of the system is a vector of all state variables: $x_t = [x_1(t),...,x_n(t)]$. The change in any state vector in time can be predicted from the current and past causal interactions among system's elements. This can be defined by a set of ordinary differential equations.

$$\begin{aligned} &\frac{dx_1}{dt} = f_1(x_1, x_2, ..., x_n) \\ &... \\ &\frac{dx_n}{dt} = f_n(x_1, x_2, ..., x_n) \end{aligned} \quad \Rightarrow \quad \frac{dx}{dt} = \begin{bmatrix} f_1(x) \\ ... \\ f_n(x) \end{bmatrix} = F(x) \qquad (2\text{-}1) \quad (57)$$

In order to specify the f_i in the formula above, a set of parameter θ is needed. The function f_i also depends upon the input to the system. Therefore the changes in the state variables caused by these inputs (u) evolve temporally depending upon the pattern of interaction among system's elements (57). The equation above should therefore be modified as follows:

$$\frac{dx}{dt} = \begin{bmatrix} f_1(x_1,...,x_n,u,\theta_1) \\ ... \\ f_n(x_1,...,x_n,u,\theta_n) \end{bmatrix} = F(x,u,\theta) \qquad (2\text{-}2) \quad (57)$$

The model provided by this equation describes the causal interactions of the system elements and external inputs of a dynamic system in time. One assumption in the model above is that the inputs (u) are independent from each other; otherwise, the relation among inputs should be further explained by a differential equation like equation 2-1 (57).

If the brain is considered as a system, the different cortical regions can be regarded as system elements, whose causal interactions we wish to understand. The input vector *u* would then be the experimental manipulations, such as sensory inputs or changes in instructions (e.g., attention). DCM, which is a system-based hypothesis-driven application, is described in the next section.

Section 2-3: Dynamic Causal Modeling

In this approach the brain is described as a multiple input - multiple output system where the inputs correspond to experimental manipulations and outputs are the regional brain responses measured by neuroimaging techniques such as the fMRI-derived regional blood oxygenation-dependent (BOLD) signal. The causal interactions among cortical areas are parameterized in order to explain the regional BOLD measurements obtained by the scanner. DCM utilizes a causal model by which neuronal activity in a given region causes

changes in neuronal activity in other regions in the model (via a pattern of interregional connections) and in its own activity by local self-regulatory connections (58). Additionally, any of these connections can be modulated by sensory inputs and contextual variables, such as a cognitive set (e.g. attention) implemented in the experimental design (58). The system's parameters are not known, thus in brief DCM is a **system identification** procedure using a Bayesian scheme to estimate the parameters associated with each connection in the hypothesized model.

DCM implements two models to test a causal hypothesis. The first is a **model of neural dynamics** that takes into account the intrinsic connectivity among various regions and the modulation in connectivity in response to experimental manipulations. This model constitutes the hypothesis. The second model is a **hemodynamic model,** which translates neural activity to hemodynamic response. The algorithm starts with a prior range that the parameters are likely to lie within and the aim of DCM is to adjust both the dynamic and hemodynamic parameters of the model in an iterative manner such that the estimated BOLD signals are maximally similar to the experimentally measured BOLD signals. The estimated parameters are then used to infer the strength of connection among the modeled regions.

Details of the Dynamic Causal Technique are reviewed in greater depth below, in sections that discuss the neuronal dynamic model (Section 2-3-1) and the hemodynamic model that relates neuronal activity to BOLD signal (Section 2-3-2).

Section 2-3-1: Description of the neuronal dynamic model in DCM

DCM implements a differential equation to describe the neural dynamics in a system of L interacting cortical regions. The neural state vector $Z = [Z_1 ... Z_L]$ describes the neuronal states at each region. The neuronal states are not direct neurophysiological

measurements but they characterize the mean activity of a region's entire neuronal population (57).

The "hidden" neural dynamics can then be defined by any differential equation:

$$\dot{z} = F(z, u, \theta) \qquad (2\text{-}3) \qquad (55)$$

F is a nonlinear function that expresses the influence induced upon each region by activity z in all L brain regions and by external input u. θ , is the parameter set of the model, which has to be estimated and whose value is required to infer the strength of coupling among regions.

The Taylor expansion of Equation 2-3 would be:

$$\frac{dx}{dt} = f(x,u) \approx f(x_0,0) + \frac{\partial f}{\partial x}x + \frac{\partial f}{\partial u}u + \frac{\partial^2 f}{\partial x \partial u}ux + \ldots \qquad (2\text{-}4)$$

If we neglect the higher order terms, equation 2-4 would be simplified as:

$$\frac{dz}{dt} = (A + \sum_{j=1}^{m} u_j B^{(j)})z + Cu \qquad (2\text{-}5) \qquad (55)$$

$$A = \frac{\partial \dot{z}}{\partial z} \qquad B^{(j)} = \frac{\partial}{\partial u_j}\frac{\partial \dot{z}}{\partial z} \qquad C = \frac{\partial \dot{z}}{\partial u}$$

Where u_j is the j^{th} input (either stimulus or cognitive set) that enters the system and propagates through interregional connections. Matrix A contains fixed connectivity among the modeled regions, which is intrinsic to the network of areas and exists in the baseline condition of the experimental design. However, since it is a state that is changed as a function of the experimental manipulations, this intrinsic coupling may be specific to each experiment (55) and dependent on the context of experimental design. $B^1, \ldots, B^m$

parameterize the modulation of intrinsic connections by any experimental manipulations. Lastly matrix C depicts the strength of direct driving inputs to the modeled system (e.g., sensory stimulus). The units of all parameters are in hertz (HZ), and thus the inference for strong connection relates to an influence that is expressed quickly in time (55). $\theta_C = [A, B_j, C]$ is the connectivity or coupling matrix that constitute the hypothesis and we wish to identify.

A main conceptual aspect of DCM concerns the ways experimental inputs should enter the model and cause neuronal responses. Based on the description of dynamics of the interacting regions, the inputs can cause responses in one of two ways (56):

1) They can act directly on some specific anatomical regions, as specified in matrix C.

2) They can evoke a response through modulation of coupling among different anatomical regions, as specified in matrix B.

It is interesting to note that conventional analysis of fMRI data (e.g., GLM) supposes that all inputs have direct access to all brain regions. Thus, conventional analysis assumes that activations observed in all regions are caused directly by experimental inputs, whereas in DCM analysis the modeler specifies the regions in which the inputs might apply their direct effect and how that effect might be propagated by modulation in the intrinsic connectivity pattern.

To further demonstrate how the underlying neuronal response in each region (z) is estimated according to this model, an example is given in Figure 2-1. This figure shows an hypothesis of a network comprising of 5 regions ($z1$ to $z5$) with 2 inputs ($u1$ and $u2$). Input 1, is a stimulus acting directly on region 1, while the 2nd input which is a cognitive set, modulates the connection from region 2 to 4 as well as region 3 to 2.

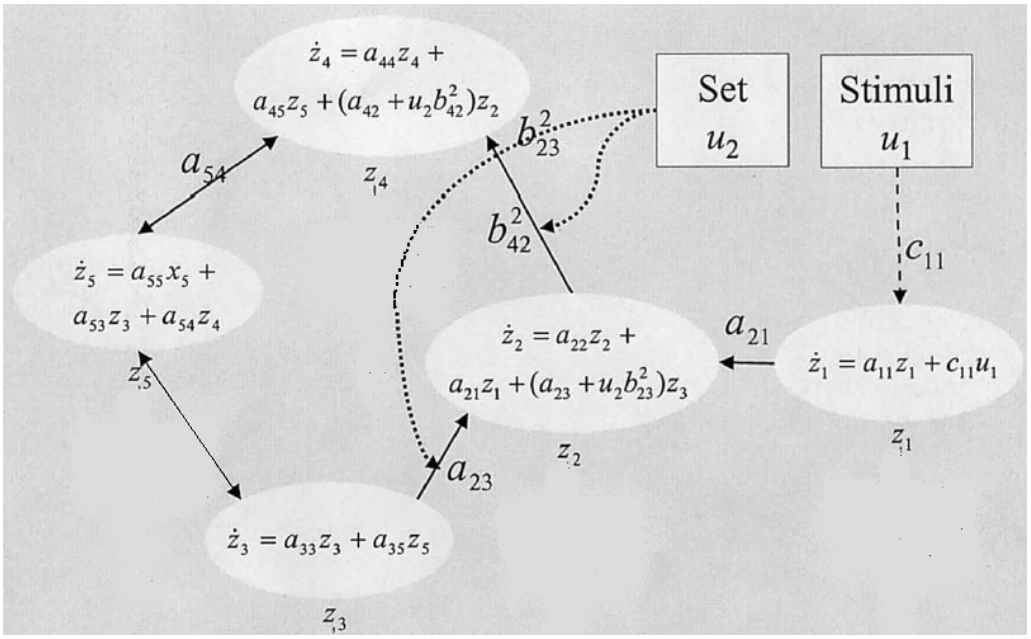

Figure 2-1. Model of neural dynamic (55) (figure is taken with permission)

Therefore in Equation 2-6 below (written in a matrix format) the non-zero elements in matrix A, B, and C specify the modeler's hypothesis about the structure of the neural network involved. In this way the modeler decides which connections are likely to be present, where the modulation is expected to act, and where it is probable for the direct effect of inputs to exert an effect. After estimation of the parameters, which is discussed in section 2-4, a statistical method is used to determine which of the modeled connections (parameters) are necessary and sufficient to evoke the observed BOLD response.

$$\begin{bmatrix} \dot{z}_1 \\ . \\ . \\ . \\ \dot{z}_5 \end{bmatrix} = \left\{ \begin{bmatrix} a_{11} & \cdots & \cdots & 0 \\ a_{21} & a_{22} & a_{23} & \cdots \\ \cdots & \cdots & a_{33} & \cdots a_{35} \\ \cdots & a_{42} & \cdots a_{44} & a_{45} \\ 0 & \cdots & a_{53} a_{54} & a_{55} \end{bmatrix} + u_2 \begin{bmatrix} 0 & \cdots & \cdots & 0 \\ \cdots & \cdots & b_{23}^{\,2} & \cdots \\ \cdots & \cdots & \cdots & \cdots \\ \cdots & b_{42}^{\,2} & \cdots & \cdots \\ 0 & \cdots & \cdots & 0 \end{bmatrix} \right\} \begin{bmatrix} z_1 \\ . \\ . \\ . \\ z_5 \end{bmatrix} + \begin{bmatrix} c_{11} & 0 \\ . & \\ . & \\ . & \\ 0 & \cdots \end{bmatrix} \begin{bmatrix} u_1 \\ u_2 \end{bmatrix} \qquad (2\text{-}6)$$

Section 2-3-2: Hemodynamic model in DCM

As we are dealing with fMRI data, the neuronal activity in each region described in the previous section should be translated to a hemodynamic signal. Therefore the model describing the neuronal dynamic should be combined with another model that relates the neuronal activity with the BOLD signal. The hemodynamic model used in DCM is basically a Single Input Single Output (SISO) system with neuronal activity z as input and the BOLD signal as output. This biophysical model describes the physiological changes accompanying neuronal activation.

The hemodynamic signal is an indirect measurement of the neural activity. It is a consequence of a series of indirect effects relating to the changes in some physiological factors (59): 1) changes from neuronal activity z to the changes to cerebral blood flow f; 2) changes in f to changes in cerebral blood volume v; 3) changes in f and v to changes in cerebral oxygen consumption rate; and 4) changes in oxygen consumption rate leading to the changes in the venous deoxyhemogolobin content q. There are 4 equations with 5 hemodynamic parameters in total that describe this model which are discussed by Stephan et al in (60).

Section 2-4: Rephrasing the problem in the Bayesian Inference Scheme

Based on the combined neurodynamic and hemodynamic model, the BOLD signal of each region can be predicted if the values of the coupling parameters are known. According to the Bayesian scheme, the value of the connectivity and hemodynamic parameters (θ_C, θ_H) is initialized at some prior range, which is empirically derived. These constraints which are defined with a Gaussian distribution (called a prior distribution), eventually form a posterior distribution according to **Bayes' Rule**. Subsequently, the

parameters are updated through an iterative procedure, so as to minimize the difference between the predicted and actual time courses. The inference about the intrinsic or modulatory connectivity is based on the posterior density that is obtained according to Bayesian estimation.

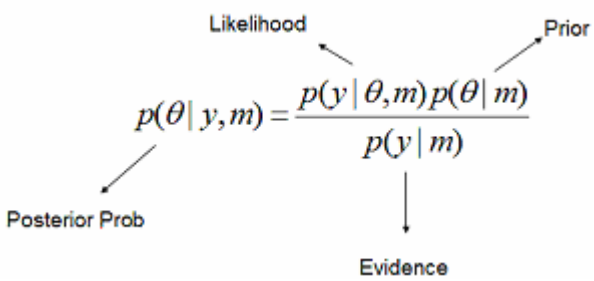

(2-7) (58)

In the equation above, y stands for data, m for model and θ for parameter. The parameter vector which we are aiming to identify is $\theta = [\theta_C, \theta_H]$. The next section provides a short description of the priors in DCM followed by a discussion of the maximization algorithm used for the estimation of the Posterior distribution.

Section 2-4-1: Priors

Based on the constraints that are described in this section, a prior distribution for each connection in A and B_j and C is assigned, which takes the form of a normal distribution. $\theta_C = [A, B_j, C]$ is the connectivity or coupling matrix that we wish to identify.

$$p(A_{ik}) = N(0, v_a)$$

$$p(B_{ik}^j) = N(0, v_b)$$

$$p(C_{im}) = N(0, v_c)$$

1-Prior on the self connections

In DCM, one assumption is that the self connections for all brain regions have the same prior probability distribution (56). According to the neurodynamic model in DCM, the neural signal decays with an exponential function. As discussed by Friston (56), the prior distribution for the self-connection is constrained to have a half-life of approximately 500 ms, falling in the range of 300 ms to 2 s (The time required for the neural signal to reaches half of its total duration is called the half-life of neural transient.). This is shown in Figure 2-2.

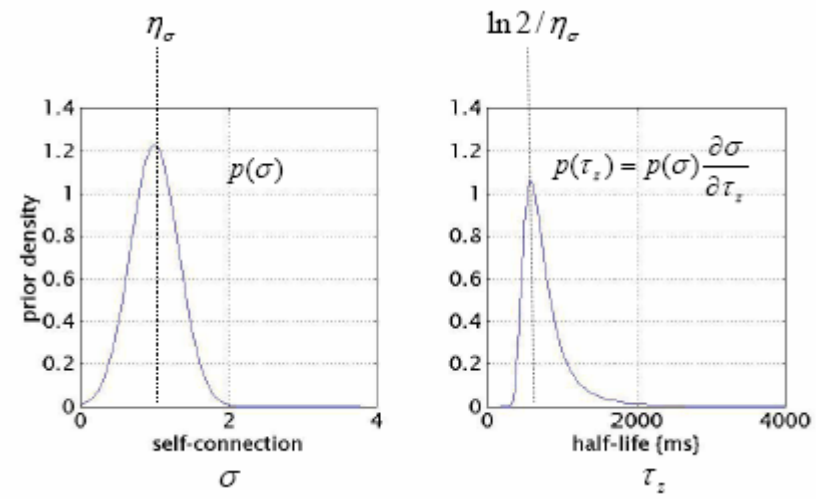

Figure 2-2. Prior distribution of self connection (56) (figure is taken with permission)

2-Priors for the stability of the system

It is evident that neuronal activity cannot diverge to infinite values. Therefore in the absence of inputs, the dynamic must return to a stable mode. The prior variance v_a is set to guarantee stability (58). The coupling parameters have a prior distribution with zero mean (58), so the value of the posterior parameters would shrink towards zero (the mean), based on the prior variance v_a (58).

3-Hemodynamic priors

The mean and variance of the 5 hemodynamic parameters, have been empirically derived (56).

Table 2-1. Prior on biophysical parameters (56) (table is taken with permission)

Parameter	Description	Prior mean η_θ	Prior variance C_θ
κ	rate of signal decay	0.65 per sec	0.015
γ	rate of flow-dependent elimination	0.41 per sec	0.002
τ	hemodynamic transit time	0.98 sec	0.0568
α	Grubb's exponent	0.32	0.0015
ρ	resting oxygen extraction fraction	0.34	0.0024

Section 2-4-2: Estimation of the parameter posteriors

As mentioned previously, according to Bayes' rule, the posterior distribution is equal to the likelihood times the prior divided by evidence (m stands for model),

$$p(\theta \mid y, m) = \frac{p(y \mid \theta, m).p(\theta \mid m)}{p(y \mid m)} \qquad (2\text{-}8) \qquad (58)$$

Taking logs gives:

$$l = \log p(\theta \mid y, m) = \log p(y \mid \theta, m) + \log p(\theta \mid m) - \log p(y \mid m) \qquad (2\text{-}9)$$

The parameters that maximize the objective function l can be found using a Gauss-Newton optimization scheme (58). The goal of this optimization is to estimate the mean

and covariance of the posterior density. This posterior density is required to infer about the strength of the connections.

Section 2-4-3: Hyper parameters of the error covariance

Error covariance should consist of what is left over after everything has been explained by the model. But since the algorithm starts with priors and then moves to the posterior density that minimizes the error, it is obvious that until the very last iterations, error covariance might perhaps consist of some patterns. In other words, when the model does not match the data completely, the error is not random noise, but can instead be written in terms of specific parameters.

One very simple example of hyper-parameters is when $Cov(\varepsilon) = \sigma^2 I$. In this case, error covariance does not consist of noise but rather has a variance of σ. In DCM, the error covariance is assumed to have the following form:

$$Cov(\varepsilon) = \lambda_1 Q_1 + \lambda_2 Q_2 + ... + \lambda_k Q_k \qquad (2\text{-}10) \quad (56)$$

Where variance components Q model the error through some hyper parameters λ.

Section 2-4-4: Expectation Maximization Algorithm (EM)

The optimization procedure which is discussed by Penny et al in (58) is called the EM algorithm and consists of 2 steps. In the **E step**, the mean and covariance of the parameters are being updated while the hyper-parameters of the error covariance are kept constant, and in the **M step,** the mean and covariance of the parameters are kept constant and the hyper-parameters are updated (58). The model parameters are initialized to the mean of the prior distribution and the EM procedure is performed iteratively until the maximum posterior density of the parameters (the most likely parameters, given the data) is obtained (58).

Section 2-4-5: Interpretation of the result

The posterior probability density of the parameters $p(\theta \mid y, m)$, given the data (y) and model (m), is thus obtained through the EM algorithm. After each parameter is characterised by a Gaussian distribution with a mean (η_θ) and covariance, its mean can be compared statistically against a chosen threshold γ. This threshold can be chosen as a function of the expected half-life of the neural process (e.g. $\gamma = (\ln 2) / \tau$) (61). Therefore, using one model, the modeler can say with what probability a parameter exceeds the threshold. Usually, a 90% confidence threshold is used to infer that a specific connection exists in the model.

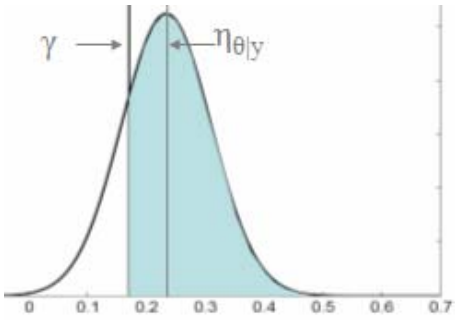

Figure 2-3-posterior probability density

Section 2-5: Comparison of different models

Within the framework of the Bayesian scheme, the modeler can compare the competing hypotheses and conclude which of the several alternative models is optimal, given the data. Basically the comparison between the 2 models is decided using the Bayes factors. Given models $m = i$ and $m = j$, the Bayes factors comparing model i to model j are defined as the ratio of model evidences (58):

$$B_{ij} = \frac{p(y \mid m = i)}{p(y \mid m = j)} \qquad (2\text{-}11)$$

Where $p(y \mid m = j)$ is the evidence for model j .

It has been discussed by Penny et al (58) that, as in classical statistics a cut-off value of 0.05 is conventionally used ($p<0.05$); likewise some threshold (Bayes Factor of 3) is used in DCM analysis for model comparison. The table below is used for the interpretation of the Bayes factors comparing one model versus the other.

Table 2-2. Interpretation of Bayes Factors (58) (table is taken with permission)

Interpretation of Bayes factors

B_{ij}	$p(m = i\|y)$ (%)	Evidence in favor of model i
1–3	50–75	Weak
3–20	75–95	Positive
20–150	95–99	Strong
≥150	≥99	Very strong

Bayes factors can be interpreted as follows. Given candidate hypotheses i and j, a Bayes factor of 20 corresponds to a belief of 95% in the statement 'hypothesis i is true'. This corresponds to strong evidence in favor of i.

There are different criteria for comparing the competing hypotheses and deciding which model provides the best explanation of the data. An absolute model fit is one of the criteria often taken into account when assessing model goodness. However, in order to get the smallest possible error (absolute model fit), the number of parameters in the model should be increased, resulting in increased model complexity and therefore over-fitting the data. This notion is depicted in the Figure 2-4. Thus, in order to explain the data properly there should be an optimal balance between accuracy and complexity.

The model evidence can be decomposed into 2 terms: accuracy, which quantifies model fit, and complexity, which explains the redundancy of model parameters.

$$\log p(y \mid m) = Accuracy(m) - Complexity(m) \qquad (2\text{-}10) \qquad (58)$$

Since there is no analytical solution for model evidence, approximations are required (58). For DCM the two approximations that are often used are: Bayesian Information Criterion (BIC) and Akaike Information Criteria (AIC) (58).

The best model (The one with the highest evidence) should show a good compromise between accuracy and complexity. This is depicted by the middle graph in the Figure 2-4 below. Generally, BIC favors simple models, while AIC favors complex models (58); this can lead to disagreement between the two. Penny et al. (58) have suggested a conservative strategy, which is to calculate the Bayes factors according to BIC and AIC criterion and to make a final decision if both factors agree (58).

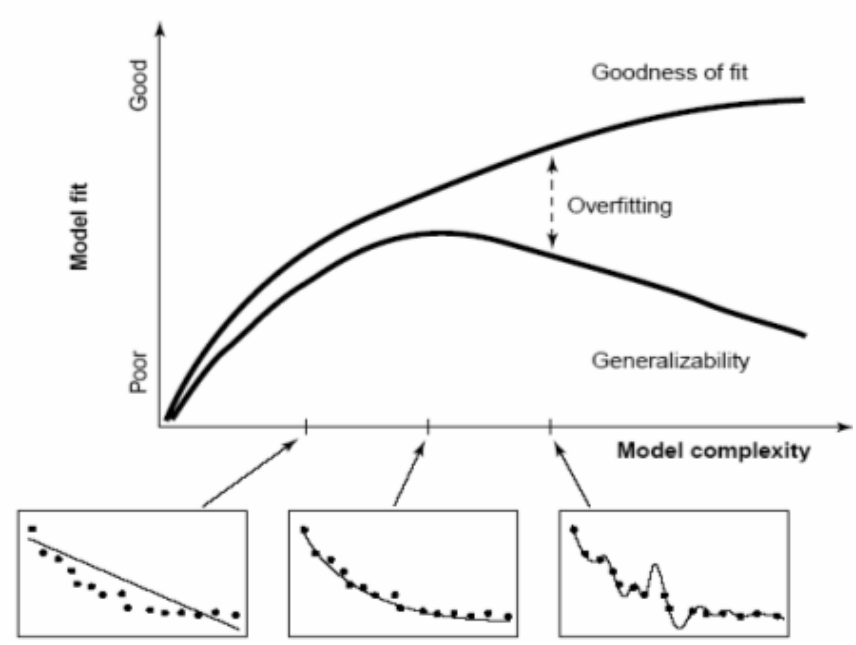

Figure 2-4. Model fit versus model complexity (65) (figure is taken with permission)

Chapter 3- Hypotheses

This chapter summarizes all hypotheses that were tested in this study. In total, we performed 3 series of modeling. Series #1 included bilateral S1 and S2 (4-Region network), series #2 included only contralateral S1 and bilateral S2 (3-Region network), and series #3 contained only contralateral S1 and S2 (2-Region network).

Section 3-1 describes the 12 hypotheses for the 4-Region network, which includes the intrinsic, modulatory and extrinsic connectivity patterns of activity. Since not all subjects showed bilateral activation in S1 and S2, additional models were tested including 3-Region and 2-Region networks (see section 3-2).

Section 3-1: Hypotheses for 4-Region network

With the aim of testing causal hypotheses of interactions between S1 and S2 in the context of pain, we systematically tested a set of 12 models of integration between S1 and S2, including inter- and intra-hemispheric connections, using data recorded while subjects were receiving painful stimuli (electric shock) on their right leg. We divided our models into 4 categories based on candidate locations of pain modulation within the modeled systems. The following subsections contain a description of the intrinsic connectivity pattern, as defined for our DCM analysis (section 3-1-1), a discussion of the 4 categories based on where modulation may occur within the intrinsic network (section 3-1-2), and a discussion of the extrinsic influence of painful stimulation for the 3 models per category (section 3-1-3).

Section 3-1-1: Intrinsic Connectivity

Because of the reciprocal nature of inter-hemispheric connections through the corpus callosum, we assumed the presence of a reciprocal callosal connection between

homologous regions of S1 and S2 in all the models that we tested for intrinsic connectivity (Figure 3-1). Furthermore, since the anatomical relation between S1 and S2 has been well established, we also assumed reciprocal connections between S1 and S2 within each hemisphere. (The self-connection in each region is one of the assumptions of DCM: see Chapter 2 for discussion).

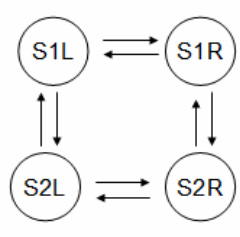

Figure 3-1. Intrinsic Connectivity

Section 3-1-2: Modulatory Connectivity

We tested 4 categories of models based on where we hypothesized that pain would modulate the intrinsic connectivity pattern. In the Category 1 we tested the hypothesis that only the left (contralateral) side of the network (S1L-S2L) would be modulated during the period that subjects were receiving painful stimuli. This modulatory effect is depicted by the blue arrows in the Figure 3-2. Since self-connection is one of the assumptions of DCM, we assumed that the modulation of pain would also influence the self-connections in all categories.

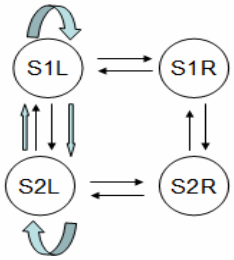

Figure 3-2. Category 1- Modulatory Connectivity (Black lines represent the intrinsic network and Blue lines represent the modulatory connectivity)

For Category 2, we added S2L-S2R reciprocal modulatory connectivity to that described in Category 1 (with self modulatory connectivity in S2R). We systematically added S1R-S2R for Category 3 and S1L-S1R for Category 4. Thus Category 4 consists of a model in which modulation occurs everywhere in the intrinsic network (Figure 3-3).

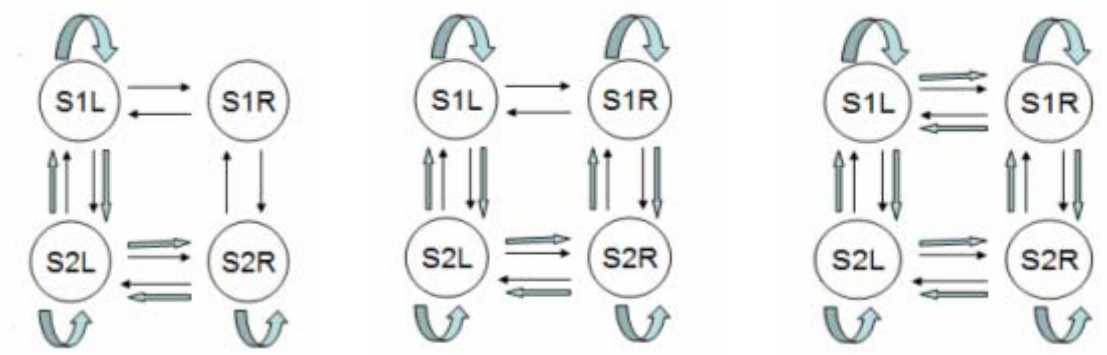

Figure 3-3. Modulatory connectivity: Category 2, Category 3, and Category 4 (from left to right respectively)

The value of a modulatory parameter is added to the value of the intrinsic connection it refers to. Therefore, a negative modulatory value means that there is a context or sensory-specific reduction in the strength of the endogenous connection.

Section 3-1-3: Extrinsic connectivity

Each of the 4 categories consists of 3 models in which we tested where the direct effect of the nociceptive stimulus would enter the model. In a conventional General Linear Model (GLM) analysis it is assumed that the external input has direct access to all regions in the brain, whereas in causal modeling we can test this directly by modeling all possible cases. The first model hypothesized a direct effect of pain only in S1L, whereas in the second model, we hypothesized a direct effect of pain in S1L and S2L. In the third model, we tested direct input to S1L, S2L and S2R; therefore this model directly tested whether the

thalamo-cortical input to S2 is redundant, given the input coming from S1, or if it is indeed necessary to explain the data. This driving effect of the pain stimulus is depicted with a red arrow in Figure 3-4 which shows one of the 12 tested models: model 1, category 1. All 12 models in the 4-Region network hypothesis are depicted in figure 3-5

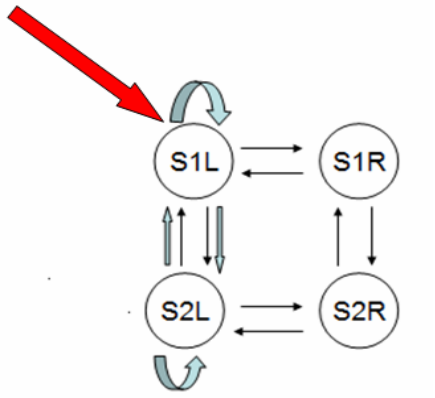

Figure 3-4. Model 1 of Category 1

Section 3-2: All the Models Tested

This section provides a summary of all the series of modeling. Eleven subjects participated in the study, and three levels of stimulation were applied: Level-3 (moderately painful), Level-2 (slightly painful), and Level-1 (non-painful). Details about the stimulation paradigm and the 3 levels of stimulation are provided in chapter 4 (Methods). In order to test a series of connectivity models we extracted the regional time courses based on the criteria that are described in section 4-5. If no voxel met these criteria for one of the regions during a subject's functional run, that subject was excluded from the 4-Region network DCM analysis. Since not all subjects showed bilateral activation in S1 and S2, additional models were tested including 3-Region and 2-Region network (see below).

Series #1: 4-Region network

For the Level-3 pain dataset, all 4 regions were clearly activated across all subjects, however, for the Level-2 pain condition there was no activity for S1R for 2 subjects, and for the Level-1 run, S1R activity was not observed in many subjects. We therefore tested the 4-Region network hypothesis for both Level-3 (11 subjects) and Level-2 pain sessions (9 subjects), but not for the Level-1 condition. The 12 models for this series of modeling have already been described in section 3-1 and depicted in figure 3-5.

Series #2: 3-Region network

In order to confirm whether S1R contributes to a prediction of responses of the regions in the network or if it simply introduces redundant information, we also tested a series of 3-Region network hypothesis (excluding S1R) for all the functional runs. This resulted in 6 possible models per subject (see Figure 3-6).

Series #3: 2-Region network

As will be shown in Chapter 5, for the Level-1 stimulus condition a bayesian comparison across the six models in the 3-Region network did not provide any winning model, which may suggest that S2R provides unnecessary information for response estimation across the network, for this dataset. Since fMRI activity was also relatively weak for the ipsilateral sites for both S1 and S2 (low t-values in the GLM results), we tested a series of 2-Region network for only the Level-1 stimulus condition by considering only contralateral regions. This resulted in 2 models per subject with inputs to S1L or both S1L and S2L. The 2-Region network hypothesis is shown in Figure 3-7.

Model 1

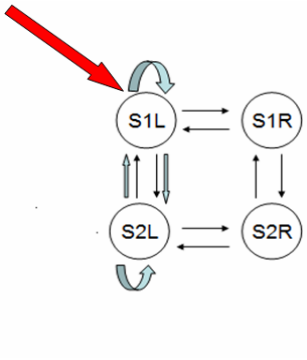

Model 2

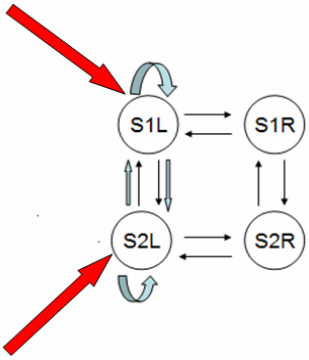

Model 3

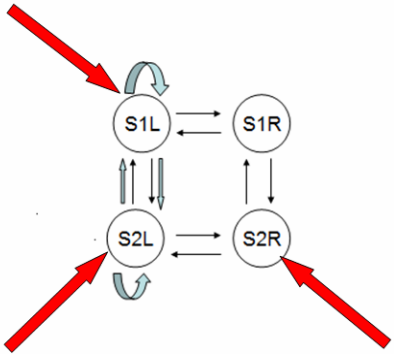

Model 4

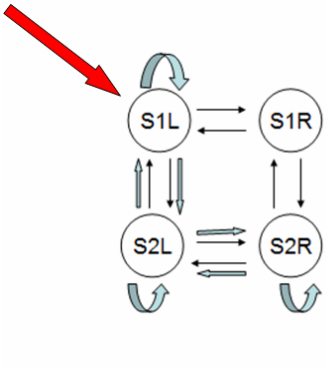

Model 5

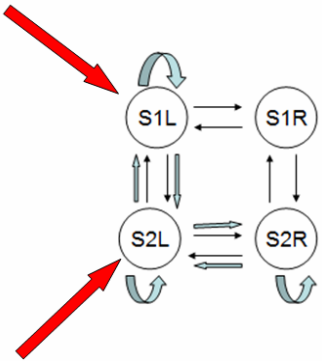

Model 6

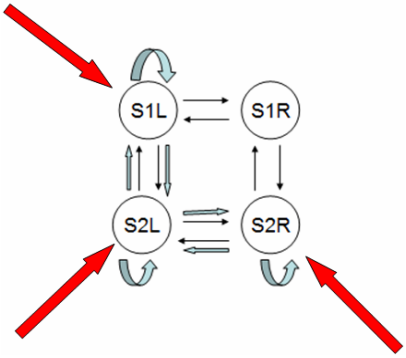

Model 7

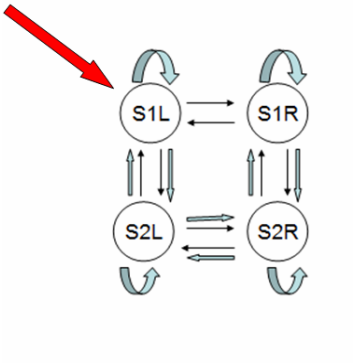

Model 8

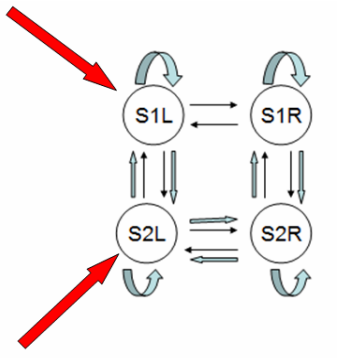

Model 9

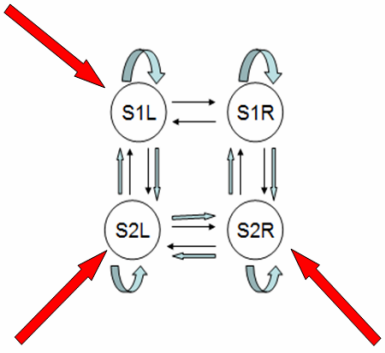

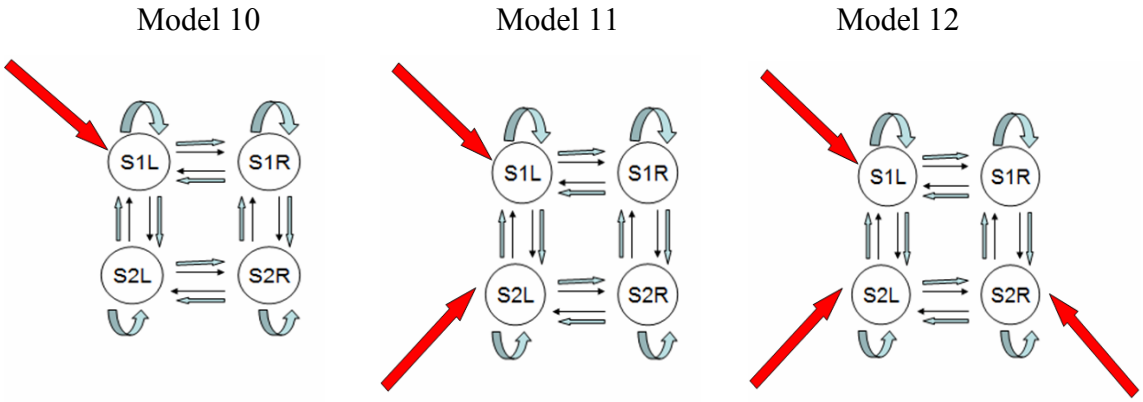

Figure 3-5. Models 1 to 12 (left to right, top to bottom) in the 4-Regions modeling; Models 1-3 belongs to Category 1, Model 4-6 belongs to Category 2, Models 7-9 belongs to Category 3, and Models 10-12 belongs to Category 4. Thin black lines represent intrinsic connectivity, Thick blue lines represent modulatory connectivity and Red lines represent extrinsic influence of pain on the network.

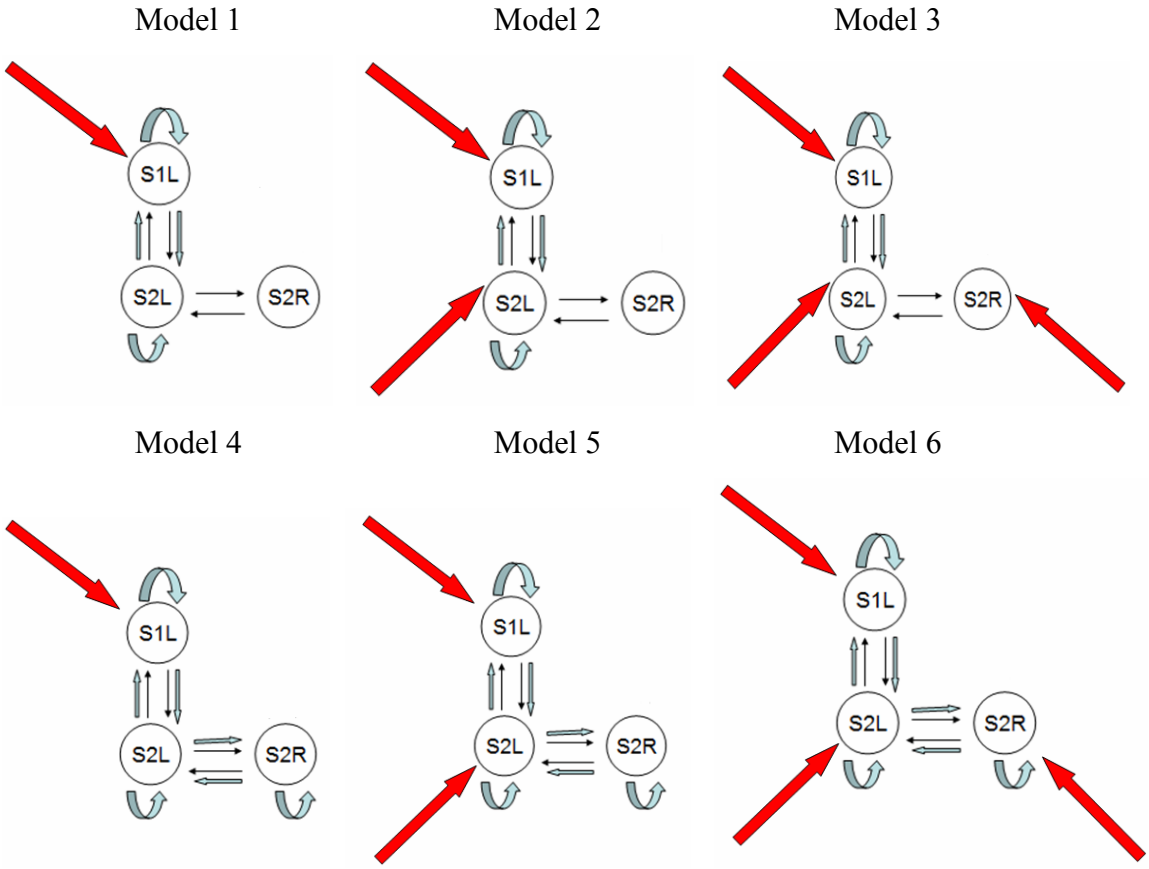

Figure 3-6. Models 1 to 6 (left to right, top to bottom) in the 3-Regions modeling; Model 1-3 belongs to Category 1, and Models 4-6 belongs to Category 2. Thin black lines represent intrinsic connectivity, Thick blue lines represent modulatory connectivity, and Red lines represent the extrinsic influence of pain on the network.

Model 1 Model 2

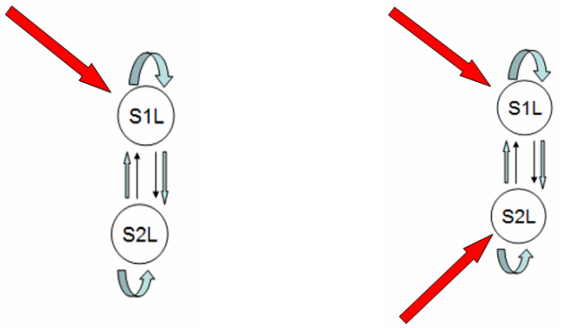

Figure 3-7. Models 1 and 2 (left to right) in the 2-Region modeling; Thin black lines represent intrinsic connectivity, Thick blue lines represent modulatory connectivity and Red lines represent the extrinsic influence of pain on the network.

Chapter 4- Methods

Section 4-1: Subjects

Eleven healthy volunteers participated in the study (three males and eight females; mean age 26.9 years; SD, 4.7). Prior to the scanning sessions, all participants were familiarized with the stimuli and the pain evaluation procedure in an MRI simulator. The Research Ethics Board of the "Centre de recherche de l'Institut de gériatrie de Montréal" approved the study. All participants gave written informed consent and received a compensation of 50$ for the brain imaging session.

Section 4-2: Stimulation Paradigm

Transcutaneous electrical stimulation was delivered with a Grass S48 square-pulse stimulator (Astro-Med Inc., West Warwick, RI, USA) connected to a custom-made constant-current stimulus-isolation unit. The stimulator was equipped with a custom-made RF filter preventing artefacts in fMRI data. The stimulation consisted of a 30 ms train of ms pulse, delivered on degreased skin over the retro-maleolar path of the right sural nerve by means of a pair of 1 custom made surface electrodes (interelectrode distance: 2 cm). Individual RIII reflex thresholds were determined using the staircase method. Stimulus-level determination and RIII reflex thresholds were performed after positioning the participant in the scanner and before the acquisition of functional images. In each functional scan, 40 stimuli were delivered with a pseudo-random ISI of 6, 9, 12 or 15s. The electrical stimuli were synchronized to the image acquisition with a script running in E-Prime (Psychology Software Tools, Inc., Pittsburgh, PA, USA).

Three levels of stimulation were applied; Level-3 (moderately painful), Level-2 (slightly painful), and Level-1 (non-painful) in a randomized order and subjects did not

perform any task during the scanning sessions. For Level-3, noxious stimulus intensity was set to 150% (mean ± SD: 15.3 ± 4.5 mA) of the RIII reflex threshold to evoke a robust RIII response, which was felt as moderately painful. For Level-2, noxious stimulation was performed at lower stimulus intensity and was set to 120% of RIII reflex threshold (12.5 ± 4.4 mA), which was felt as slightly painful. For Level-1, innocuous stimulus intensity was set to 80% of RIII threshold.

Section 4-3: fMRI acquisition parameters

Imaging data were acquired at "Unité de neuroimagerie fonctionnelle" of the "Centre de recherche de l'Institut de gériatrie de Montréal" on a 3T Siemens Trio scanner (Munich, Germany) using a CP head coil. The head of the participant was stabilized in a comfortable position using a vacuum bag. Participants were instructed to refrain as much as possible from moving throughout the imaging session and were given earplugs to reduce the noise from the scanner. The anatomical scans were T1-weighted high-resolution scans [repetition time (TR): 13 ms; echo time (TE): 4.92 ms; flip angle: 25°; field of view: 256 mm; voxel size: 1 x 1 x 1.1 mm]. The functional scans were collected using a blood oxygen level-dependent (BOLD) protocol with a T2*-weighted gradient echo-planar imaging sequence (TR: 3.0 s with an inter-volume delay of 500 ms; TE: 30 ms; flip angle: 90°; 64 x 64 matrix; 130 volume acquisitions). Electrical stimuli were always administered during the inter-volume delay, thereby avoiding any potential contamination of fMRI images by shock-induced artefacts or potential contamination of EMG recordings by RF-pulse artefacts. The scanning planes were oriented parallel to the anterior-posterior commissure line and covered the entire brain from the vertex of the cortex to the first segments of the spinal cord (41 contiguous 5-mm-thick slices; voxel size, 3.44 x 3.44 x 5 mm).

Section 4-4: GLM Analysis

The brain imaging data were analyzed using SPM2 (http://www.fil.ion.ucl.ac.uk/spm/) running in Matlab version 7.1. Pre-processing included slice-time correction and realignment. Anatomical and functional images were then spatially normalized to a standard stereotaxic space using the MNI template. Subsequently, functional images were spatially smoothed using a Gaussian kernel twice the voxel size (FWHM: 7 x 7 x 10 mm) and temporally filtered using a high-pass filter with a cut-off period of 128s. They were then corrected for serial autocorrelation using the AR(1) correction implemented in SPM. For each participant, stimulus-related activity was identified with an event-related design by convolving a vector of the onset timings for each stimulus with a canonical hemodynamic response function (hrf). The general linear model was used to model the effects of interest.

Group analyses were conducted using random-effect models with contrast images of individual-subject effects. The responses evoked by noxious stimulation were assessed by a random-effect one-sample t-test, using images of stimulus-evoked responses from each subject. This analysis provided a non-specific map of cerebral responses to noxious stimulation and confirmed that the electrical stimulus produced a brain activation pattern consistent with previous pain imaging studies.

Section 4-5: ROI definition

In a DCM analysis the first step is to extract the time-series of BOLD measurements from the regions of interest (ROIs) identified in the GLM analysis. These are the time courses that we wish to estimate based on the causal model described in chapter 2. The ROI's have been selected based on the GLM group maps and anatomical landmarks, which are discussed in this section.

The group analysis showed significant shock-evoked activation in bilateral S1 and S2. The activation maps of each individual for each stimulation level were then thresholded at $p<0.05$ to identify activated voxels within the target anatomical structures and in the vicinity of the group activation peak. The peak activation voxel in each area and for each run was selected as the center of the ROI. Time-course data were determined by the average of the first eigenvariates of the stimulus-evoked GLM responses across voxels contained within a radius of 5mm from the center of the ROI. To insure that the target regions were consistently selected across subjects, we used strict anatomical landmarks to select the ROIs (the coordinates of the ROIs of each subject are given in the Appendix). For S1, we searched for activated voxels in the putative foot area within the superior part of the post central sulcus, including the posterior part of the paracentral lobule in the medial surface of the hemisphere. For S2 we looked in the parietal operculum at the bottom of the post-central gyrus, including the posterior part of the dorsal bank of Sylvian fissure.

If no voxel met these criteria for one of the regions in a subject's functional run, that subject was excluded from the 4-Regions DCM analysis. Since not all subjects showed bilateral activation in S1 and S2, additional models were tested including 3-Region and 2-Region networks, as discussed in Chapter 3.

Section 4-6: DCM Analysis

DCM analysis was performed using SPM5 (http://www.fil.ion.ucl.ac.uk/spm/). Based on the hypotheses discussed in Chapter 3, we first specified the connectivity patterns including intrinsic, modulatory and extrinsic patterns for each of the models. For model specification, slice-time correction has also been taken into account, by entering the precise time at which each region was scanned based on the slice acquisition order, sampling time, and the spatial coordinates of each region in each subject. The next step was to make the model estimation.

For the model estimation, we used a default threshold (γ) of zero (as discussed in Section 2-4-5). This default threshold corresponds to the time of regional communication (τ) of ($\gamma = (\ln 2) / \tau$). Our aim was to test whether each connection in our model contributes to predict the regional responses. In simple terms, we asked a generic question about whether neural processing was happening at all (i.e. $\gamma > 0$) for each regional interaction that we modeled in our network. Those regional connections are represented by coupling parameters. The next step involved estimating the corresponding probability that each connection would exceed the threshold.

The 2nd level analysis evaluated whether the connections were expressed consistently across the subjects. For this we used a classical between-subjects analysis, applying a one-sample t test to the corresponding posterior estimates of each parameter across all subjects (62). Our statistical threshold was $p<0.05$. The estimated time courses for each region per subject were also extracted for the 2nd level analysis. At the next level we performed a model comparison per subject. The Bayes factors for each comparison per subject, was extracted from the Matlab output.

For model comparison, we used the BIC criterion to select the optimal model across subjects for all 3 levels of stimulation (see Chapter 5 for results). However as discussed in Chapter 2, Penny et al (58) suggest that the optimal model should have a good balance between model accuracy and complexity, and the well established BIC and AIC criteria favor simplicity and accuracy, respectively (62). Since there might be disagreement between the two criteria, they have suggested another conservative strategy, which calculates the Bayes factors associated with BIC and AIC criteria and makes a final decision only if both factors agree (58). Thus for each comparison per subject we also extracted the Bayes factors based on this conservative criterion. However, our results show that this criterion could be relied upon to make a conclusion in favor of one model only for Level-3 scans (this result is given in the Appendix, Table A-1). For Level-2 and Level-1, there was disagreement for many subjects between BIC and AIC, and thus no firm

conclusion could be made for model selection (in these cases there is no Bayes factor as the output of the model comparison, since BIC and AIC disagree). Thus, for all classes of modeling (4-Region, 3-Region and 2-Region network) we only report the BIC model comparison in the results (Chapter 5)

An established convention for favouring one model versus another is when the value of BF comparing the two is greater than 3. Thus for each subject in the group, we first computed pair-wise comparisons between all models. Since it is likely that the optimal model will vary to some degree across subjects, the decision based on Bayesian Model Selection for the group's optimal model has been made using the following 2 measures as proposed by Stephan et al (62).

1- Group Bayes Factor (GBF): A GBF has been computed across subjects by multiplying the individual BF (62). Thus the first measure for a group's optimal model is when the GBF is greater than 3.

2- Positive Evidence Ratio (PER): However, the GBF can not be relied upon if there exists strong outliers (a subject with very high BF). In such cases, an additional complementary measure has been proposed (62), which looks at whether the BF passed the threshold for positive evidence for either of the compared models. This is simply a ratio of the number of subjects that pass the BF criterion of 3 for the two compared models.

Chapter 5 – Results

Overall we tested a series of twelve 4-Region models for Level-3 and Level-2 pain sessions, a series of six 3-Region models for Level-3, Level-2 and Level-1 sessions, and finally a series of two 2-Region models only for the Level-1 dataset.

This chapter contains a description of the results of the group GLM analysis (Section 5-1), followed by the results of the optimal group model selection for the DCM analysis (Section 5-2). Section 5-3 summarizes the estimated network of the optimal group model, and Section 5-4 describes the optimal model in terms of the power of its estimation of the regional time series in the model. Lastly, the 2nd level analysis of the connectivity parameters is reviewed in Section 5-5.

Section 5-1: GLM results

In this section, the GLM results of the random effect analysis for Level-3, Level-2 and Level-1 are shown in Figures 5-1, 5-2, and 5-3 respectively. Figures 5-1 and 5-2 demonstrate the bilateral S1 and S2 activity in the group maps (threshold of 0.01, FDR corrected) for Level-3 and Level-2 pain sessions. For Level-1 (the non-painful condition), the threshold for the group t maps is 0.05 (FDR corrected) in Figure 5-3, since a threshold of 0.01 would not reveal any regional activation. However, the regional time courses have been extracted using each subject's functional t maps, based on the criteria discussed in chapter 4.

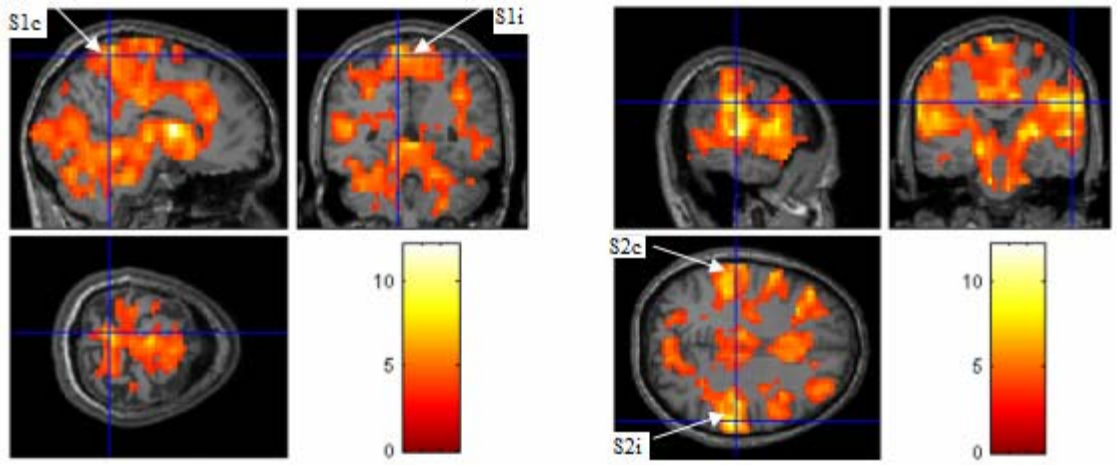

Figure 5-1. Group t-map of GLM results for Level-3 stimulation (Threshold of 0.01 FDR corrected). Arrows indicate sites of significant activation in S1 and S2, contralateral (c) and ipsilateral (i) to the stimulated site (right sural nerve).

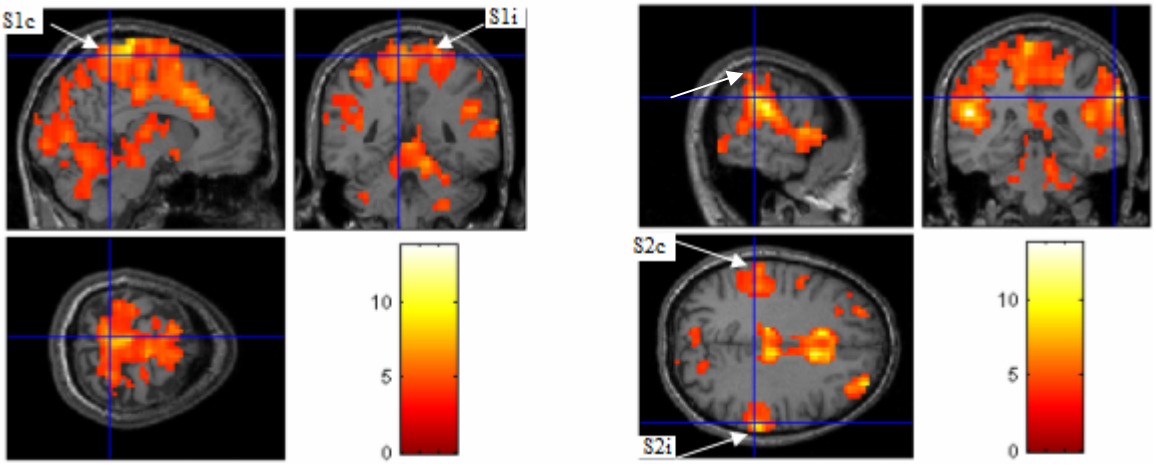

Figure 5-2. Group t map of GLM results for Level-2 stimulation (Threshold of 0.01 FDR corrected). Arrows indicate sites of significant activation in S1 and S2, contralateral (c) and ipsilateral (i) to the stimulated site (right sural nerve).

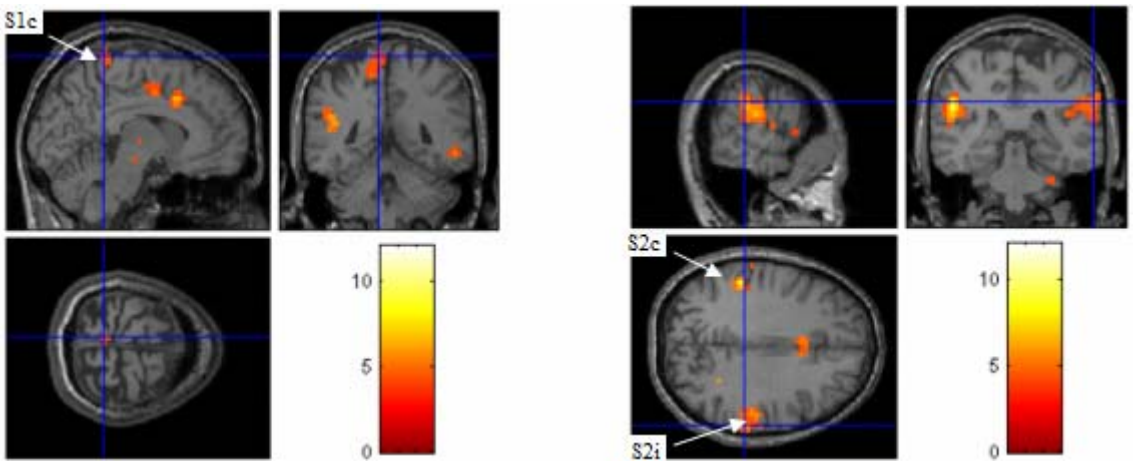

Figure 5-3. Group t map of GLM results for Level-1 stimulation (Threshold of 0.05 FDR corrected). Arrows indicate sites of significant activation in S1 and S2, contralateral (c) and ipsilateral (i) to the stimulated site (right sural nerve).

Section 5-2: Group Model Comparison

A systematic comparison of each model against every other model demonstrated that the first 3 models (Category 1) provided the best prediction of network activity (very high Bayes Factors comparing Category 1 versus the rest of the models). In this section the results of the optimal model selection for the group analysis for Level-3, Level-2 and Level-1 session are discussed in Sections 5-2-1, 5-2-2 and 5-2-3, respectively. The 2 measures, Group Bayes Factor (GBF) and the Positive Evidence Ratio (PER) (discussed in Chapter 4), have been utilized for the optimal group model selection.

5-2-1-Level-3 condition

Based on the BIC criterion, Model 1 proved to be superior across all model comparisons using the Level-3 pain dataset for both 4-Region and 3-Region modeling. This optimal group model is discussed in section 5-3. The results of this model comparison are shown in Tables 5-1 and 5-2 respectively; the majority of subjects show high Bayes factors

when comparing Model 1 to the rest of the models, which is indicative of consistency across subjects.

Table 5-1. Bayes Factors comparing Model 1 versus all the other 4-Region models, Level-3 condition. Comparison is for each subject (Subject 1-11), and across all subjects using the GBF and PER (Bayes Factors greater than 3 are highlighted) based on the BIC criterion.

Model 1 Versus	Suje 1	Suje 2	Suje 3	Suje 4	Suje 5	Suje 6	Suje 7	Suje 8	Suje 9	Suje 10	Suje 11	Group Bays Factor	PER
Model 2	17.88	36.72	9.444	0.5019	12.79	31.56	16.08	9.832	0.2369	0.33	8.809	1.37E+08	8:2
Model 3	137.1	1659	108.5	0.266	8.001	5029	112	96.72	1.506	0.02847	266.4	3.27E+16	8:2
Model 4	1439	1495	1437	1200	1048	1488	1500	1487	288.4	1342	1513	7.56E+33	11:0
Model 5	2.27E+04	1.01E+05	2.64E+04	377.8	4917	4.61E+04	1.37E+04	1.62E+04	193.3	85.26	1.38E+04	2.62E+41	11:0
Model 6	2.03E+05	2.48E+06	1.61E+05	394.1	1.18E+04	7.55E+06	1.66E+05	1.47E+05	2239	42.17	3.94E+05	2.58E+51	11:0
Model 7	2.13E+06	2.22E+06	2.13E+06	1.78E+06	1.53E+06	2.21E+06	2.22E+06	2.20E+06	4.25E+05	1.99E+06	2.24E+06	5.61E+68	11:0
Model 8	3.33E+07	1.50E+08	3.90E+07	5.55E+05	6.11E+06	6.83E+07	1.92E+07	2.40E+07	2.85E+05	1.26E+05	2.04E+07	1.52E+76	11:0
Model 9	1.87E+08	3.91E+09	2.38E+08	4.39E+05	1.01E+07	9.18E+09	1.30E+08	1.41E+08	2.88E+06	6.24E+04	5.44E+08	1.27E+85	11:0
Model 10	2.10E+08	3.39E+08	2.88E+08	7.47E+07	1.13E+08	3.96E+08	1.34E+08	2.36E+08	1.01E+06	2.65E+08	3.55E+08	2.06E+89	11:0
Model 11	2.05E+09	2.13E+10	2.21E+09	5.16E+07	4.50E+08	8.25E+09	1.16E+09	1.81E+09	2.71E+07	1.70E+07	1.97E+09	3.52E+97	11:0
Model 12	1.87E+10	5.32E+11	2.99E+10	5.27E+07	1.17E+09	4.35E+11	1.21E+10	1.86E+10	3.73E+08	8.27E+06	4.68E+10	2.59E+107	11:0

Table 5-2. Bayes Factors comparing Model 1 versus all the other 3-Region models, Level-3 condition. Comparison is for each subject (Subject 1-11) and across all subjects using the GBF and PER (Bayes Factors greater than 3 are highlighted) based on the BIC criterion.

Model 1 Versus	Suje 1	Suje 2	Suje 3	Suje 4	Suje 5	Suje 6	Suje 7	Suje 8	Suje 9	Suje 10	Suje 11	Group Bays Factor	PER
Model 2	0.9982	16.39	4.974	3.29	18.18	101.1	7.717	3.313	0.8764	1.051	27.48	3.18E+08	8:0
Model 3	12.82	520.5	8.365	8.632	10.23	3623	63.42	34.99	46.2	0.2769	1787	9.06E+17	10:1
Model 4	1442	1520	1274	1326	902.2	1483	1186	1490	693.5	241.8	1536	2.25E+33	11:0
Model 5	1334	2.92E+04	4429	3553	6536	1.39E+05	8638	4.94E+03	4314	187.7	5.38E+04	1.04E+42	11:0
Model 6	1.90E+04	7.72E+05	1.24E+04	1.28E+04	1.52E+04	5.40E+06	9.40E+04	5.18E+04	6.82E+04	408.1	2.64E+06	6.84E+52	11:0

5-2-2- Level-2 condition

As was the case for the Level-3 condition, **Model 1** proved to be superior (based on the BIC criteria) across all our model comparisons using the Level-2 pain dataset for both 4-Region and 3-Region modeling, as depicted in Tables 5-3 and 5-4, respectively. As is clear from the PER values, data from the majority of subjects agreed in favor of Model 1.

Table 5-3. Bayes Factors comparing Model 1 versus all the other 4-Region models, Level-2 condition. Comparison is for each subject (Subject 1-11), across all subjects using the GBF and PER (Bayes Factors greater than 3 are highlighted), based on the BIC criterion. (No stimulus-evoked activity was detected on the ipsilateral S1 in subjects 1 and 7 in the conventional GLM analysis with a P-value < 0.05 uncorrected)

Model 1 Versus	Suje 1	Suje 2	Suje 3	Suje 4	Suje 5	Suje 6	Suje 7	Suje 8	Suje 9	Suje 10	Suje 11	Group Ba	PER
Model 2		24.72	26.61	1.042	50.47	18.37		4.292	12.18	0.002105	1.465	1.02E+05	6:1
Model 3		0.9223	25.86	1.878	4868	34.71		3.922	4.559	0.000112	14.92	2.26E+05	6:1
Model 4		575.2	1441	1472	1499	1290		970.2	151.9	107.3	641.8	2.39E+25	9:0
Model 5		2090	2.58E+04	1292	1.06E+05	8483		1.28E+03	2943	0.1523	1309	4.70E+28	8:0
Model 6		1339	3.84E+04	2784	7.23E+06	5.14E+04		5.81E+03	6676	0.1664	2.22E+04	7.62E+33	8:0
Model 7		8.35E+05	2.13E+06	2.18E+06	2.22E+06	1.90E+06		1.44E+06	2.16E+05	1.58E+05	9.47E+05	7.61E+53	9:0
Model 8		2.56E+06	3.81E+07	1.91E+06	1.60E+08	1.23E+07		1.90E+06	2.04E+06	224.4	2.68E+07	8.55E+57	9:0
Model 9		7.00E+05	3.26E+07	3.38E+06	8.59E+09	6.32E+07		8.84E+06	2.90E+06	167.6	2.68E+07	4.82E+60	9:0
Model 10		3.34E+06	2.91E+07	1.52E+08	2.06E+08	1.79E+08		2.03E+08	3.55E+06	7.49E+06	1.82E+04	5.35E+64	9:0
Model 11		5.27E+07	1.99E+09	1.67E+08	8.79E+09	1.11E+09		2.77E+08	6.98E+07	2.05E+04	1.42E+07	9.62E+71	9:0
Model 12		5.89E+07	2.20E+09	3.59E+08	3.05E+11	6.63E+09		1.25E+09	1.41E+08	1.87E+04	1.42E+07	4.40E+75	9:0

Table 5-4: Bayes Factors comparing Model 1 versus all the other 3-Region models, Level-2 condition. Comparison is for each subject (Subject 1-11), across all subjects using the GBF and PER (Bayes Factors greater than 3 are highlighted), based on the BIC criterion.

Model 1 Versus	Suje 1	Suje 2	Suje 3	Suje 4	Suje 5	Suje 6	Suje 7	Suje 8	Suje 9	Suje 10	Suje 11	Group Bays Factor	PER
Model 2	5.562	2.927	4.578	1.492	59.94	3.148	3.097	5.13	3.828	0.0495	17.99	1.14E+06	8:1
Model 3	97.34	0.2889	2.852	5.064	1336	18.33	17.1	3.18	9.684	0.1433	5314	3.99E+12	8:2
Model 4	1495	416.6	1400	1463	1512	868.4	1418	1437	304.4	50.24	1501	7.83E+31	11:0
Model 5	8867	393.5	3575	1910	1.35E+05	2377	3513	4592	3160	113.4	2.43E+04	1.07E+39	11:0
Model 6	1.44E+05	425.1	4227	7506	1.98E+06	2.72E+04	2.53E+04	4710	1.43E+04	222.1	7.81E+06	3.09E+47	11:0

5-2-3- Level-1 condition

As mentioned earlier, many of our subjects lacked ipsilateral activation of S1 for the Level-1 condition, thus the 4-Region models could not be tested for this dataset. The group result of model comparisons for the 3-Region models for this dataset is depicted in Table 5-5. When Model 1 is compared with Model 2 and Model 3, the result is not consistent across subjects, and for many subjects no model is preferred for this comparison. Thus the group result could not provide any superior model. This leads us to exclude ipsilateral regions completely. We therefore tested a set of 2-Region models only for the Level-1 sessions. As

is shown in Table 5-6, for the 2-Region modeling, **Model 1** is superior to Model 2 except in the case of 1 subject.

Table 5-5. Bayes Factors comparing Model 1 versus all the other 3-Region models, Level-1 condition. Comparison is for each subject (Subject 1-11), across all subjects using the GBF and PER (Bayes Factors greater than 3 are highlighted), based on the BIC criterion. (No stimulus-evoked activity was detected on the ipsilateral sites in subjects 7 and 9 in the conventional GLM analysis with a P-value < 0.05 uncorrected)

Model 1 Versus	Suje 1	Suje 2	Suje 3	Suje 4	Suje 5	Suje 6	Suje 7	Suje 8	Suje 9	Suje 10	Suje 11	Group Bays Factor	PER
Model 2	3.802	0.1584	8.719	0.5126	2.66	1.589		0.9263		1.097	5.129	5.93E+01	3:1
Model 3	2.707	0.6971	1.775	0.7512	1.323	4.932		0.9847		0.2971	25.59	1.23E+02	2:1
Model 4	1047	1480	1480	1460	1200	1347		1471		1468	1482	1.73E+28	9:0
Model 5	2264	221.5	1.02E+04	510.5	1592	1415		1002		894.8	5107	2.69E+28	9:0
Model 6	4013	1033	2632	1113	1953	7310		1460		440.4	3.79E+04	4.22E+30	9:0

Table 5-6: Bayes Factors comparing Model 1 versus Model 2 (2 Regions models), Level-1 condition. Comparison is for each subject (Subject 1-11), across all subjects using the GBF and PER (Bayes Factors greater than 3 are highlighted), based on the BIC criterion. (No stimulus-evoked activity was detected on the ipsilateral sites in subjects 7 and 9 in the conventional GLM analysis with a P-value < 0.05 uncorrected.)

Model 1 Versus	Suje 1	Suje 2	Suje 3	Suje 4	Suje 5	Suje 6	Suje 7	Suje 8	Suje 9	Suje 10	Suje 11	Group Bays Factor	PER
Model 2	9.492	0.4954	12.14	4.597	3.808	7.684		15.02		4.604	8.329	4.42E+06	8:0

Section 5-3: Group results for the optimal model

This section summarizes the group results for the estimated optimal group model. As discussed in Chapter 2, after the optimal model had been selected, we computed the posterior estimates of the coupling parameters associated with each connection in the model. Those values exceeding the 90% confidence threshold were deemed significant. In this section the optimal group model in each dataset (the intrinsic and modulatory connections that exceeded the threshold) is depicted in Figures 5-4, 5-5, and 5-6, for 4-Region, 3-Region and 2-Region models, respectively

A noteworthy feature of the optimal selected model is the direct influence of the stimulation on S1L, which suggests that other inputs to S2L and S1R provide redundant

information for response estimation. As depicted in Figures 5-4 and 5-5, the patterns of connectivity are similar for 4-Region and 3-Region models for both Level-3 and Level-2 pain stimulation. It is also interesting that the patterns of intrinsic connectivity are less complex for Level-2, compared to Level-3, with Level-2 lacking the S2L to S1L intrinsic connection. The direction of the intra-hemispheric connections is also similar, which is always from the contralateral side to the ipsilateral side, and within the ipsilateral side only from S1R to S2R.

As for Level-1, which is a non-painful session, the pattern of modulatory connectivity is less complex compared to Level-3 and Level-2, with a lack of self modulatory connections for both SIL and S2L. Thus, there is a consistent increase in the degree of complexity in the network architecture from Level-1 to Level-3, a finding which accords with the idea that the more intensely painful the stimulus, the more communication there is among regions in the network, thus requiring a greater number of connections. It is also interesting to note that, with the exception of the self-modulatory connections of S1L and S2L, the only other connection that is modulated by the painful stimulation is from S1L to S2L. This is also true for the non-painful stimulation (Level-1). Thus, this result implies that the connection from S1L to S2L plays the main role in conveying noxious and innocuous inputs across the network.

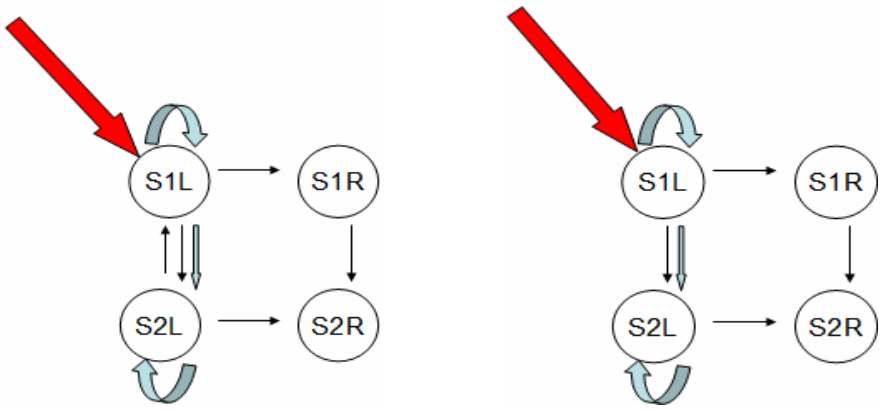

Level-3 Level-2

Figure 5-4. Optimal model for the 4-Region analysis for Level-3 and Level-2 stimulation

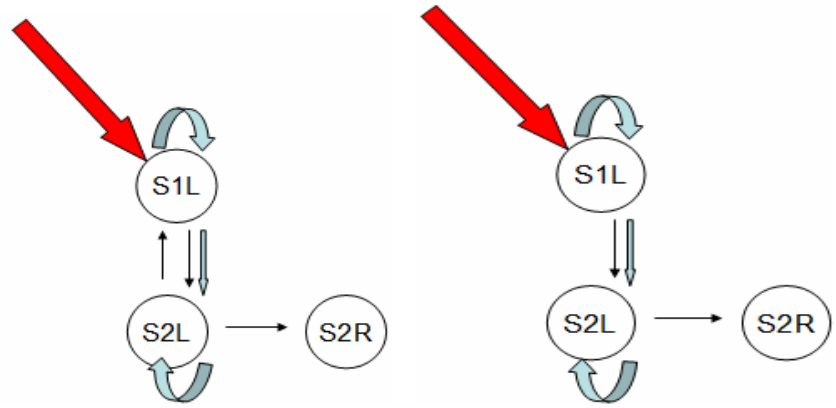

Level-3 Level-2

Figure 5-5. Optimal model for the 3-Region analysis for Level-3 and Level-2 stimulation

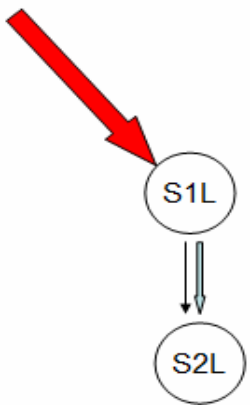

Figure 5-6. Optimal model for the 2-Region analysis for Level-1 stimulation

Section 5-4: Estimated BOLD signal

As discussed in Chapter 2, the goal of DCM analysis is to estimate the time courses of each region in the model, based on the neurodynamic and hemodynamic models by tuning the model parameters, so that the estimated time courses would be as similar as

possible to the actual time courses. In this section the results of the correlation between the estimated time courses and the actual time courses for the preferred model (Model 1) are shown to reflect the consistency in response estimation across subjects. An example of the predicted versus the actual time courses for the four regions is depicted in Figure 5-7.

The results for the correlation between the estimated and actual time courses across subjects and for all 3 level of stimulation are shown in Tables 5-7 to 5-11. Non-significant values ($p<0.05$) are noted as "*n.s.".

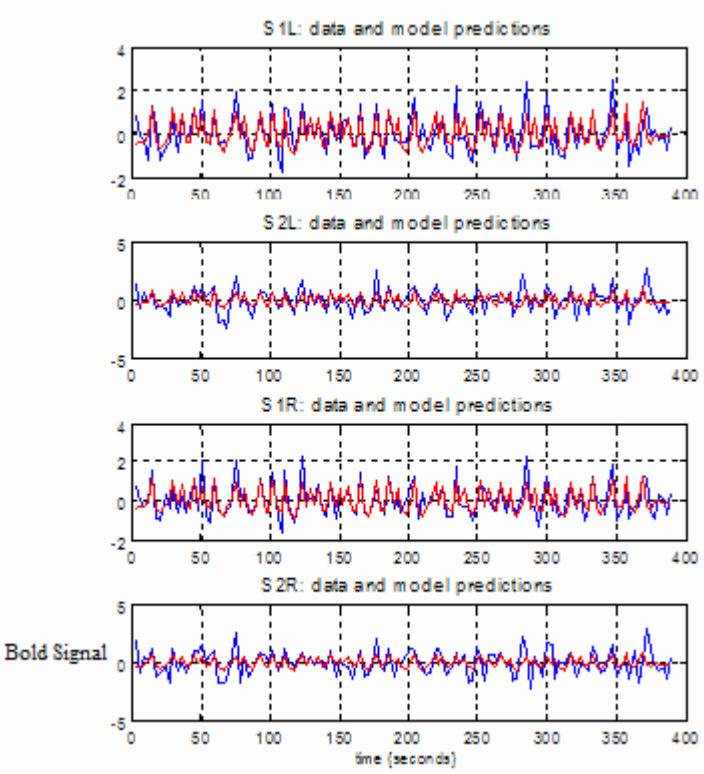

Figure 5-7. Observed (Blue) Vs Predicted (Red) time course for the 4-Region Model-1 in subject 1 (Level-1 dataset)

Level-3 Condition

For Level-3 scans in the 3-Region models, none of the subjects exceeds the threshold of 0.05; but in the 4-Region models, only subjects 4 and 10 failed to reach the threshold of 0.05 for S1R and S2R, respectively.

Table 5-7. Corr Coef- 4-Region models Level-3 condition (Non-significant values ($p<0.05$) are noted as "*n.s.")

Subject #	S1L	S2L	S1R	S2R
Suje 1	0.4473	0.4713	0.3534	0.4285
Suje 2	0.5013	0.4431	0.5118	0.5025
Suje 3	0.535	0.383	0.472	0.4195
Suje 4	0.4417	0.3783	0.1564 * n.s.	0.4689
Suje 5	0.6843	0.4143	0.5091	0.49
Suje 6	0.5421	0.4242	0.4649	0.48
Suje 7	0.4014	0.5452	0.343	0.3597
Suje 8	0.7161	0.5151	0.7731	0.5118
Suje 9	0.4489	0.6992	0.4013	0.484
Suje 10	0.471	0.3411	0.2406	0.161 * n.s.
Suje 11	0.7848	0.6246	0.7335	0.6089

Table 5-8. Corr Coef- 3-Region models

Subject #	S1L	S2L	S1R
Suje 1	0.4448	0.468	0.4284
Suje 2	0.5036	0.441	0.5024
Suje 3	0.5295	0.381	0.4209
Suje 4	0.4422	0.3776	0.4691
Suje 5	0.6871	0.4144	0.4873
Suje 6	0.5502	0.4256	0.4807
Suje 7	0.4008	0.5453	0.36
Suje 8	0.7225	0.5103	0.5084
Suje 9	0.4438	0.7003	0.495
Suje 10	0.4643	0.3624	0.3347
Suje 11	0.7887	0.6251	0.6127

Level-2 Condition

For the Level-2 sessions, all the correlations for all the subjects attained the significance threshold of 0.05, except for one case; Subject 4, S1R (Tables 5-9 and 5-10).

Table 5-9. Corr Coef- 4-Region models Level-2 Condition (Non-significant values ($p<0.05$) are noted as "*n.s.")

Subject #	S1L	S2L	S1R	S2R
Suje 2	0.5094	0.432	0.4614	0.3876
Suje 3	0.5169	0.3118	0.3129	0.304
Suje 4	0.3356	0.2597	0.1263 *n.s.	0.2754
Suje 5	0.6686	0.4605	0.7188	0.5014
Suje 6	0.6406	0.5107	0.428	0.4681
Suje 8	0.5967	0.4566	0.5459	0.4172
Suje 9	0.4979	0.5969	0.4704	0.4202
Suje 10	0.6793	0.5951	0.4487	0.2309
Suje 11	0.6847	0.5784	0.5901	0.515

Table 5-10. Corr Coef- 3-Region models

Subject #	S1L	S2L	S1R
Suje 1	0.4743	0.4546	0.3583
Suje 2	0.5094	0.4316	0.3804
Suje 3	0.5182	0.3093	0.2899
Suje 4	0.3359	0.259	0.2753
Suje 5	0.6655	0.459	0.4929
Suje 6	0.6432	0.5094	0.4767
Suje 7	0.3836	0.3126	0.246
Suje 8	0.596	0.4417	0.4381
Suje 9	0.5	0.5974	0.4293
Suje 10	0.6781	0.6054	0.3328
Suje 11	0.6854	0.5794	0.5223

Level-1 Condition

For the Level-1 condition, all correlations in all subjects were significant, with the exception of two cases; S1L for Subject 11 and S2L for Subject 3 (Table 5-11).

Table 5-11. Corr Coef- 2-Region models, Level-1 Condition (Non-significant values ($p<0.05$) are noted as "*n.s.")

Subject #	S1L	S2L
Suje 1	0.3567	0.3808
Suje 2	0.2526	0.207
Suje 3	0.2564	0.1581 * n.s.
Suje 4	0.3007	0.2131
Suje 5	0.557	0.431
Suje 6	0.3031	0.2447
Suje 8	0.3536	0.2794
Suje 10	0.2973	0.2059
Suje 11	0.1422 * n.s.	0.2002

Section 5-5: Second Level analysis of model parameters

Once the optimal model was selected, we next tested the consistency of the modeled connections across subjects. We therefore have done a classical between-subject analysis by performing a one sample t test to posterior estimates of the intrinsic and modulatory parameters across subjects. For these second-level analyses, we adopted a threshold of p-uncorrected < 0.05. The results for all classes of modeling are summarized in this section.

4-Region models

For the Level-3 stimulus condition in the 4-Region models, no parameters failed to meet the significance threshold of $p<0.05$. This means that the values associated with all connections from the 1st level analysis (group posterior estimates; section 3-5) were expressed consistently across subjects. Thus, the 2nd level analysis for the Level-3 condition confirms the group posterior estimate shown in Figure 5-4.

For the Level-2 stimulation, the only connection in the group posterior estimate that failed to reach the significance threshold of 0.05 was the intrinsic connection S1L-S2L (the non significant values are highlighted in the tables). This means that not all the subjects had the same intrinsic parameter associated with this connection.

Table 5-12. Intrinsic and Modulatory Connectivity Parameters (4-Region models) from left to right. Mean and Standard Deviation (STD) of the intrinsic and modulatory parameters across subjects, and the t test across each parameter. Those values that did not reach the threshold of 0.05 are highlighted.

Level 3					
	S1L-S2L	S1L-S1R	S2L-S1L	S2L-S2R	S1R-S2R
Mean	0.2826	0.4238	-0.0686	0.3599	0.2574
STD	0.1687	0.1687	0.1687	0.1687	0.1687
Pval	0.0002	0.0000	0.0139	0.0000	0.0001

Level 2				
	S1L-S2L	S1L-S1R	S2L-S2R	S1R-S2R
Mean	0.1163	0.3793	0.3301	0.1959
STD	0.1929	0.1929	0.1929	0.1929
Pval	0.1081	0.0000	0.0001	0.0043

Level 3			
	S1L	S1L-S2L	S2L
Mean	0.0334	0.2799	0.0570
STD	0.0382	0.1613	0.0575
Pval	0.0158	0.0002	0.0082

Level 2			
	S1L	S1L-S2L	S2L
Mean	0.0560	0.3250	0.0636
STD	0.0618	0.1799	0.0548
Pval	0.0264	0.0006	0.0083

3-Region models

In the 3-Region modeling for the Level-3 condition, the only existing connection in the group posterior estimate that failed to reach the significance threshold of 0.05 was the S1L self modulatory connection. For the Level-2 condition, in the intrinsic network, S1L-S2L and in the modulatory network, only the S1L self-modulatory connection failed to reach statistical significance.

Table 5-13. Intrinsic and Modulatory Connectivity Parameters (3-Region models) from left to right. Mean and Standard Deviation (STD) of the intrinsic and modulatory parameters across subjects, and the t test across each parameter. Values that did not reach the threshold of 0.05 are highlighted.

Level 3			
	S1L-S2L	S2L-S1L	S2L-S2R
Mean	0.3514	-0.1211	0.6072
STD	0.2486	0.2486	0.2486
Pval	0.0009	0.0090	0.0000

Level 2		
	S1L-S2L	S2L-S2R
Mean	0.1801	-0.5098
STD	0.2903	0.2903
Pval	0.0667	0.0000

Level 3			
	S1L	S1L-S2L	S2L
Mean	0.0272	0.3974	0.1002
STD	0.0505	0.1658	0.0784
Pval	0.1037	0.0000	0.0017

Level 2			
	S1L	S1L-S2L	S2L
Mean	0.0375	0.4207	0.1021
STD	0.0772	0.2004	0.0857
Pval	0.1383	0.0000	0.0027

2-Region models

In the 2-Region modeling for the Level-1 stimulus dataset, all the connections in the group posterior estimate (depicted in figure 5-6) except the self-modulatory connection in S1L, were expressed consistently across subjects.

Table 5-14. Intrinsic and Modulatory Connectivity Parameters (2-Region modesl) from left to right. Mean and Standard Deviation (STD of the intrinsic and modulatory parameters across subjects, and the t test across each parameter. Values that did not reach the threshold of 0.05 are highlighted.

Level 1	
	S1L-S2L
Mean	0.3132
STD	0.1473
Pval	0.0002

Level 1			
	S1L	S1L-S2L	S2L
Mean	-0.0030	0.2631	0.0365
STD	0.0106	0.1491	0.0469
Pval	0.4211	0.0007	0.0480

Chapter 6- Discussion and conclusion

The goal of causal modeling is to obtain information about the neuronal network that supports a perceptual aspect of a cognitive function. Since S1 and S2 are believed to be implicated in the sensory discriminative aspect of pain perception, we tested the interactions between these regions in the context of pain. The serial or parallel processing within the somatosensory cortex is a debatable issue which we tried to address in this study. We also tackled the issue of hemispheric transfer of information within the somatosensory cortex, which has not been studied by any causal modeling approach. Our paradigm consisted of 3 runs with intensity changing from non painful (Level-1) to slightly painful (Level-2) and lastly to a moderately painful session (Level-3). Therefore our paradigm allowed us to investigate how the intensity of a cutaneous stimulus is encoded in our network of interest, and how the modulation of regional connections in response to our experimental stimulation would differ across conditions. Our results show a difference between painful and non-painful conditions, with the non-painful condition demonstrating connectivity between only contralateral somatosensory regions, while the painful conditions showed clear evidence of connectivity both within and between contralateral and ipsilateral somatosensory areas.

Section 6-1-1: Serial versus parallel processing scheme

As shown in Figures 5-4 to 5-6 in Chapter 5, the superior model has only a direct sensory input to the left primary somatosensory cortex (S1L), contralateral to the site of stimulation; this implies that parallel inputs to the secondary somatosensory cortices (S2L and S2R) provide redundant information for response estimation. This means that, based on the causal model utilized for studying the dynamics of the system (as described in Chapter 2), the direct input to S1L is sufficient for the estimation of time series in our network of

interest, which is in accordance with the serial mode of processing. It is important to note that our result does not rule out the possibility that thalamocortical projections convey nociceptive information to S2, but it suggests that although S2 might receive direct input from thalamus, this input does not contribute to information processing within our network of interest in the context of our paradigm. However if our stimulation paradigm changes, for example if we incorporate the simultaneous application of noxious electrical and thermal stimulation, the demand for more information processing may require the contribution of existing thalamocortical projections to S2 in the causal interactions among regions.

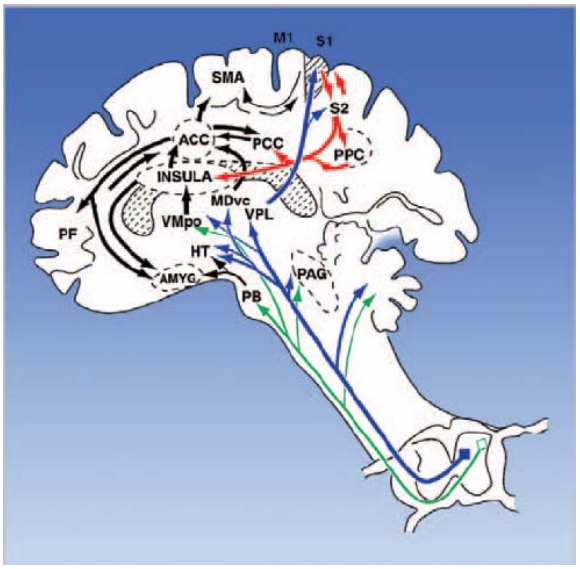

Figure 6-1. Ascending pain pathways (1) (figure is taken with permission)

A potential limitation of this study, which will be discussed in section 6-2, is the limited number of regions that can be included in DCM modeling. As discussed in Chapter 1, pain is a multidimensional experience with different areas devoted to processing different components of the experience. Thus if the experimental paradigm manipulates different aspects of pain, such as unpleasantness or expectation, different pain areas might

be more or less active depending on their function. For example, the insula and ACC are important areas that are implicated in the affective dimension of pain. Price's model of nociceptive processing (Figure 6-1) indicates that both insula and ACC receive projections from S2. So, we might speculate that if these pain areas were included in our model and if the experimental paradigm were to manipulate pain unpleasantness rather than intensity, then other input to S2 might play a crucial role in response estimation.

Section 6-1-2: Inter-hemispheric communication in somatosensory regions

Our results show inter-hemispheric connection from the contralateral to ipsilateral side, which suggest that the electrical stimulation first activated the contralateral side and that the information was then conveyed to the ipsilateral hemisphere, likely through callosal fibers. This finding is consistent with anatomical studies ((11),(12)) that showed the existence of inter-hemispheric callosal pathways. It is interesting to reflect that the direction of information flow from the side contralateral to the stimulation to the opposite hemisphere is in accordance with major anatomical pathways.

Studies on callostomized and split-brain patients ((50), (53), (52), (51)), show bilateral S1 and S2 activation, which implies the existence of some compensatory mechanism, likely through direct thalamocortical projections to the ipsilateral hemisphere. Again our result simply implies that although this compensatory pathway might exist in normal subjects, the information provided by this pathway is redundant and secondary to the information coming from the contralateral side.

Section 6-1-3: Increase in network complexity during pain

The intrinsic coupling, which forms the connectivity in the baseline condition, is a state that is specific to each experiment and perturbed as a result of experimental manipulations (55). Regarding intrinsic connectivity, our results show that during the

Level-3 stimulus condition there is a reciprocal connection between S1 and S2 in the contralateral hemisphere. This reciprocal connection between S1 and S2 has been confirmed by anatomical ((11),(12)), ablation ((37),(40),(39),(36)), and evoked-potential studies ((44),(30),(42)) as discussed in Chapter 1, so our result is consistent with previous work on S1-S2 interactions. It is also interesting to note that as the intensity of the painful stimulus is reduced from Level-3 to Level-2, the complexity of the network is also reduced, with only an intrinsic connection from S1 to S2 in Level-2 rather than a reciprocal connection.

As regards modulatory connectivity, our results indicate that pain only modulates the contralateral pathways – the S1L-S2L connection as well as self-connections on S1L and S2L. As discussed in Chapter 1, response-latency studies ((44),(30),(42)) have shown that S2 is activated later than S1, indicating that S2 is higher on the hierarchy of pain processing than S1. This implies that the information flow should be from S1 to S2, which is consistent with our findings. For the pain conditions (Level-3 and Level-2), the pattern of modulatory connectivity was identical, but for the non-painful condition (Level-1), a similar pattern was observed but with a lack of self-modulatory connections in S1 and S2. Like the intrinsic connectivity, we observed an increase in the complexity of causal interactions from the non-painful to the painful conditions for the modulatory connectivity. This finding is reasonable, since the pain condition activates both nociceptive and non-nociceptive fibers, while in the non-painful condition the nociceptive fibers have not been activated by the electrical stimulation. So a less complex cortical network is the result of a smaller amount of information being conveyed in the non-painful condition compared to the pain condition.

Moreover, pain is a more complex sensory modality with many perceptual dimensions. Different components of pain interact with each other, for example, the emotional component can alter the sensory component and vice versa (63). Thus, as the noxious stimulus induces an emotional response, there should be accordingly more

complexity in the neuronal network to support the enhanced processing required by the emotional event, compared to the non-painful condition. In the visual system it has been shown by Vuilleumier et al (64) that a lesion in the amygdala eliminates the enhanced activation that typically occurs in the visual cortex in response to emotional facial expressions. The amygdala plays a central role in emotional regulation and has many connections with different areas, including the visual and somatosensory areas. It has been argued (64) that the increase in neuronal activity in visual areas in normal subjects reflects the higher demand on perceptual analysis caused by the feedback connection from amygdala. Making an analogous comparison with the visual system, we might therefore hypothesize that the emotional component of the pain stimulus would require a boost in the perceptual processing, likely through causal connections from emotional processing regions like the amygdala to somatosensory areas. The flow of this extra information to the somatosensory regions compared to the nonpainful condition would require more processing in these areas, which supposedly would be reflected by more causal interaction among these regions.

Overall, our results favour the serial mode of processing noxious information, and the intrinsic pattern that we hypothesized in our network accords with previous studies on S1-S2 interactions and transcallosal connections. Our results shed new light on causal influences within the somatosensory areas, by showing that the modulation of pain occurs in the S1-S2 connection as well in as self-connections in S1 and S2 within the contralateral hemisphere. Our results also show a more complex neuronal network in the somatosensory regions that reflects the enhanced demand for information processing required by the noxious compared to the innocuous stimulus.

Section 6-2: Limitations

DCM considers the brain as an input-output system. By disturbing the system with designed inputs, measured BOLD responses (outputs) are used to estimate the various

parameters that govern the evolution of brain states (neuronal activity in each region). As discussed in Chapter 2, DCM utilizes two models for estimating the unknown parameters. The first model is a neuronal model of interacting cortical regions with neurophysiologically meaningful parameters. This neuronal model tries to describe how the neuronal responses are caused. Effective connectivity is turned into parameters in terms of connections among brain regions; causality is inherent in the equations that characterize the model. However since our knowledge of the brain's dynamic is limited, future investigation should increase the accuracy of the model as well as refine the description of the causal influences of one region upon another. The second model is a biophysical model of the neurovascular responses that convert the neural dynamics into hemodynamics. Although this model has been validated by physiological experiments, the assumptions underlying this model need further consideration (60), and the exact relation between a neurophysiological process and the resulting BOLD response remains unknown.

A further drawback to the neural dynamic model is the limitation to the number of regions that can be included in the models. Published work on DCM usually includes 3 to 4 regions in each model. Validation studies show that DCM does not provide a good estimate of regional time courses when the number of regions in the model exceeds five. For this reason we did not add more regions like the insula, ACC or PFC in our model, and we did not test a network including all pain regions. DCM still needs a more precise dynamic model of regional interactions when the number of regions is more than five. However future studies examining the dynamics of the brain should help us to apply DCM to more regions in the pain matrix, for example, testing the interactions between S1, S2, ACC, and insula as described by Price (1) in figure 6-1.

Another limitation of DCM, is its temporal resolution. Two factors place a limitation on DCM modelling in this regard: the TR (Repetition Time) of any acquisition does not match the neurophysiological timing of the neuronal responses, and the hemodynamic model and the parameters inherent in the biophysical model are empirically

derived. Another potential timing problem for the application of DCM is the temporal shift between regional time series because of multi-slice acquisition. This problem has been corrected in SPM5, which permits the timing that each region has been scanned to be entered according to the slice acquisition order.

Lastly, the main limitation of our pain paradigm was the presentation of different stimulus intensities in different scanning sessions rather than in a single session. Here we analyzed the results of the 3 sessions separately and compared them qualitatively. Presenting the 3 levels of intensity in a random order in a single session would have allowed us to look at the contrast between them and to compare them quantitatively. However the disadvantage of a random paradigm would have been the difficulty in analyzing differences in intrinsic connectivity across sessions, especially those resulting from clear cognitive differences between the subject's expectations of pain and non-pain conditions.

Section 6-3: Future directions

As discussed by Friston ((55, 56)), the best experimental design for DCM is a multifactorial design with at least one factor controlling sensory-evoked responses and another factor manipulating the context in which the effects of the sensory-evoked responses are propagated throughout the system. This contextual factor can modulate the latent or intrinsic coupling among areas.

A future design well suited to DCM analysis would be a block design with separate blocks of heat pain, randomly presented, in which subjects would be instructed to direct their attention towards or away from the pain stimulus. This design would permit the contrast between attended versus unattended blocks to examine which connections are modulated by this cognitive variable. Other cognitive manipulations like suggestion (26) can also be implemented in a block design. For example another potential study would be

to investigate the difference between suggestion and attentional modulation in a network including ACC, S1 and S2, with one session consisting of attentional modulation and another session controlling suggestion towards increasing or decreasing pain.

One of the main findings of this study was the hemispheric transfer of information from the left hemisphere (contralateral to the stimulation site) to the homologous regions within the ipsilateral hemisphere. It would be interesting test whether the direction of transcallosal connections are dependent on hemispheric dominance. This can be simply implemented in a randomly distributed group of left- and right-hand subjects by an event-related or block design, where the stimulation site would randomly change from left to right. Since callosal connections are believed to be denser in the midline structures, one future design well suited for this investigation would be a random application of electrical stimulation or heat pain to the trunk or face. Another future study in this line of investigation could be DCM modeling in the same network of S1 and S2, conducted in split-brain and callosotomized patients, in order to assess connectivity relationships associated with the bilateral stimulus-related BOLD responses observed in some of these patients in the absence of direct inter-hemispheric connections. By including left and right sensory thalamus within DCM models, one could test the hypothesis that these sub-cortical (and spinal pathways) convey information to the ipsilateral hemisphere in the absence of inter-hemispheric fibers.

Conclusion

We implemented a causal modeling approach to study the integration among bilateral somatosensory areas S1 and S2 in the context of pain. Our Paradigm consisted of 3 scanning sessions with intensity changing from non painful (Level-1) to slightly painful (Level-2) and lastly to a moderately painful session (Level-3), which allowed us to investigate how the intensity was encoded in our network of interest, and how the modulation of regional connections by our experimental stimulation would differ across conditions. We tested a series of hypotheses assessing how nociceptive input is relayed and propagated within our network of interest. Our hypotheses tackled three questions; first the issue of serial versus parallel processing in the somatosensory cortex, second the hierarchical relationship between S1 and S2, and lastly inter-hemispheric connections of the homologous somatic sensory areas.

Among the various models tested, the optimal model contradicted the notion of parallel processing, implying that parallel inputs to S2L and S2R provide redundant information for response estimation and do not contribute to processing the information in our network of interest, in the context of our paradigm. For both intrinsic and modulatory connectivity we observed an increase in the complexity of causal interactions from nonpainful to painful condition. The optimal model indicates modulation in the S1-to-S2 connection, which suggests that S2 is higher on the hierarchy of pain processing than S1, in accordance with previous neurophysiological and MEG findings. Lastly, conventional functional imaging studies often show bilateral somatosensory activation, but cannot reveal the direction of information flow between hemispheres. Results from our DCM analysis of the functional data support the anatomical evidence that suggested the entrance of somatosensory information into the hemisphere contralateral to the stimulation side, with inter-hemispheric connections responsible for the transfer of information to the ipsilateral hemisphere.

Bibliographie

1. Price DD. Central neural mechanisms that interrelate sensory and affective dimensions of pain. Mol Interv. 2002 Oct;2(6):392-403, 339.

2. Bushnell MC, Duncan GH, Hofbauer RK, Ha B, Chen JI, Carrier B. Pain perception: is there a role for primary somatosensory cortex? Proc Natl Acad Sci U S A. 1999 Jul 6;96(14):7705-9.

3. Apkarian AV, Bushnell MC, Treede RD, Zubieta JK. Human brain mechanisms of pain perception and regulation in health and disease. Eur J Pain. 2005 Aug;9(4):463-84.

4. Almeida TF, Roizenblatt S, Tufik S. Afferent pain pathways: a neuroanatomical review. Brain Res. 2004 Mar 12;1000(1-2):40-56.

5. Schnitzler A, Ploner M. Neurophysiology and functional neuroanatomy of pain perception. J Clin Neurophysiol. 2000 Nov;17(6):592-603.

6. Kandel ER, Schwartz JH, Jessell TM. Principles of neural science. 4th ed. New York ; Montréal: McGraw-Hill Health Professions Division; 2000.

7. Kenshalo DR, Jr., Chudler EH, Anton F, Dubner R. SI nociceptive neurons participate in the encoding process by which monkeys perceive the intensity of noxious thermal stimulation. Brain Res. 1988 Jun 28;454(1-2):378-82.

8. Kenshalo DR, Jr., Giesler GJ, Jr., Leonard RB, Willis WD. Responses of neurons in primate ventral posterior lateral nucleus to noxious stimuli. J Neurophysiol. 1980 Jun;43(6):1594-614.

9. Duncan GH, Albanese MC. Is there a role for the parietal lobes in the perception of pain? Adv Neurol. 2003;93:69-86.

10. Murray EA, Mishkin M. Relative contributions of SII and area 5 to tactile discrimination in monkeys. Behav Brain Res. 1984 Jan;11(1):67-83.

11. Jones EG, Powell TP. Connexions of the somatic sensory cortex of the rhesus monkey. I. Ipsilateral cortical connexions. Brain. 1969;92(3):477-502.

12. Jones EG, Powell TP. Connexions of the somatic sensory cortex of the rhesus monkey. II. Contralateral cortical connexions. Brain. 1969;92(4):717-30.

13. Potagas C, Avdelidis D, Singounas E, Missir O, Aessopos A. Episodic pain associated with a tumor in the parietal operculum: a case report and literature review. Pain. 1997 Aug;72(1-2):201-8.

14. Greenspan JD, Winfield JA. Reversible pain and tactile deficits associated with a cerebral tumor compressing the posterior insula and parietal operculum. Pain. 1992 Jul;50(1):29-39.

15. Ploner M, Freund HJ, Schnitzler A. Pain affect without pain sensation in a patient with a postcentral lesion. Pain. 1999 May;81(1-2):211-4.

16. Greenspan JD, Lee RR, Lenz FA. Pain sensitivity alterations as a function of lesion location in the parasylvian cortex. Pain. 1999 Jun;81(3):273-82.

17. Dong WK, Hayashi T, Roberts VJ, Fusco BM, Chudler EH. Behavioral outcome of posterior parietal cortex injury in the monkey. Pain. 1996 Mar;64(3):579-87.

18. Apkarian AV, Stea RA, Bolanowski SJ. Heat-induced pain diminishes vibrotactile perception: a touch gate. Somatosens Mot Res. 1994;11(3):259-67.
19. Bolanowski SJ, Maxfield LM, Gescheider GA, Apkarian AV. The effects of stimulus location on the gating of touch by heat- and cold-induced pain. Somatosens Mot Res. 2000;17(2):195-204.
20. Talbot JD, Marrett S, Evans AC, Meyer E, Bushnell MC, Duncan GH. Multiple representations of pain in human cerebral cortex. Science. 1991 Mar 15;251(4999):1355-8.
21. Jones AK, Brown WD, Friston KJ, Qi LY, Frackowiak RS. Cortical and subcortical localization of response to pain in man using positron emission tomography. Proc Biol Sci. 1991 Apr 22;244(1309):39-44.
22. Apkarian AV, Stea RA, Manglos SH, Szeverenyi NM, King RB, Thomas FD. Persistent pain inhibits contralateral somatosensory cortical activity in humans. Neurosci Lett. 1992 Jun 22;140(2):141-7.
23. Timmermann L, Ploner M, Haucke K, Schmitz F, Baltissen R, Schnitzler A. Differential coding of pain intensity in the human primary and secondary somatosensory cortex. J Neurophysiol. 2001 Sep;86(3):1499-503.
24. Carrier B, Rainville P, Paus T, Duncan GH, MC B. Attentional modulation of pain-related activity in human cerebral cortex. Soc Neurosci Abstr. 1998;24:1135.
25. Hofbauer RK, Rainville P, Duncan GH, Bushnell MC. Cortical representation of the sensory dimension of pain. J Neurophysiol. 2001 Jul;86(1):402-11.
26. Rainville P, Carrier B, Hofbauer RK, Bushnell MC, Duncan GH. Dissociation of sensory and affective dimensions of pain using hypnotic modulation. Pain. 1999 Aug;82(2):159-71.
27. Rainville P, Duncan GH, Price DD, Carrier B, Bushnell MC. Pain affect encoded in human anterior cingulate but not somatosensory cortex. Science. 1997 Aug 15;277(5328):968-71.
28. Chen JI, Ha B, Bushnell MC, Pike B, Duncan GH. Differentiating noxious- and innocuous-related activation of human somatosensory cortices using temporal analysis of fMRI. J Neurophysiol. 2002 Jul;88(1):464-74.
29. Iwamura Y. Hierarchical somatosensory processing. Curr Opin Neurobiol. 1998 Aug;8(4):522-8.
30. Inui K, Wang X, Tamura Y, Kaneoke Y, Kakigi R. Serial processing in the human somatosensory system. Cereb Cortex. 2004 Aug;14(8):851-7.
31. Iwamura Y, Iriki A, Tanaka M. Bilateral hand representation in the postcentral somatosensory cortex. Nature. 1994 Jun 16;369(6481):554-6.
32. Duffy FH, Burchfiel JL. Somatosensory system: organizational hierarchy from single units in monkey area 5. Science. 1971 Apr 16;172(980):273-5.
33. Iwamura Y. Bilateral receptive field neurons and callosal connections in the somatosensory cortex. Philos Trans R Soc Lond B Biol Sci. 2000 Feb 29;355(1394):267-73.
34. Taoka M, Toda T, Iriki A, Tanaka M, Iwamura Y. Hierarchical organization of bilateral neurons in the second somatosensory cortex of awake macaque monkeys. Soc Neurosci Abstr. 1998b;24:1381.

35. Fitzgerald PJ, Lane JW, Thakur PH, Hsiao SS. Receptive field (RF) properties of the macaque second somatosensory cortex: RF size, shape, and somatotopic organization. J Neurosci. 2006 Jun 14;26(24):6485-95.

36. Murray GM, Zhang HQ, Kaye AN, Sinnadurai T, Campbell DH, Rowe MJ. Parallel processing in rabbit first (SI) and second (SII) somatosensory cortical areas: effects of reversible inactivation by cooling of SI on responses in SII. J Neurophysiol. 1992 Sep;68(3):703-10.

37. Turman AB, Morley JW, Zhang HQ, Rowe MJ. Parallel processing of tactile information in cat cerebral cortex: effect of reversible inactivation of SII on SI responses. J Neurophysiol. 1995 Mar;73(3):1063-75.

38. Turman AB, Ferrington DG, Ghosh S, Morley JW, Rowe MJ. Parallel processing of tactile information in the cerebral cortex of the cat: effect of reversible inactivation of SI on responsiveness of SII neurons. J Neurophysiol. 1992 Feb;67(2):411-29.

39. Garraghty PE, Pons TP, Kaas JH. Ablations of areas 3b (SI proper) and 3a of somatosensory cortex in marmosets deactivate the second and parietal ventral somatosensory areas. Somatosens Mot Res. 1990;7(2):125-35.

40. Burton H, Sathian K, Shao DH. Altered responses to cutaneous stimuli in the second somatosensory cortex following lesions of the postcentral gyrus in infant and juvenile macaques. J Comp Neurol. 1990 Jan 15;291(3):395-414.

41. Pons TP, Garraghty PE, Mishkin M. Serial and parallel processing of tactual information in somatosensory cortex of rhesus monkeys. J Neurophysiol. 1992 Aug;68(2):518-27.

42. Inui K, Wang X, Qiu Y, Nguyen BT, Ojima S, Tamura Y, et al. Pain processing within the primary somatosensory cortex in humans. Eur J Neurosci. 2003 Nov;18(10):2859-66.

43. Salami M, Itami C, Tsumoto T, Kimura F. Change of conduction velocity by regional myelination yields constant latency irrespective of distance between thalamus and cortex. Proc Natl Acad Sci U S A. 2003 May 13;100(10):6174-9.

44. Kitamura Y, Kakigi R, Hoshiyama M, Koyama S, Watanabe S, Shimojo M. Pain-related somatosensory evoked magnetic fields following lower limb stimulation. J Neurol Sci. 1997 Feb 12;145(2):187-94.

45. Kakigi R, Hoshiyama M, Shimojo M, Naka D, Yamasaki H, Watanabe S, et al. The somatosensory evoked magnetic fields. Prog Neurobiol. 2000 Aug;61(5):495-523.

46. Killackey HP, Gould HJ, 3rd, Cusick CG, Pons TP, Kaas JH. The relation of corpus callosum connections to architectonic fields and body surface maps in sensorimotor cortex of new and old world monkeys. J Comp Neurol. 1983 Oct 1;219(4):384-419.

47. Jones EG, Hendry SH. Distribution of callosal fibers around the hand representations in monkey somatic sensory cortex. Neurosci Lett. 1980 Sep;19(2):167-72.

48. Iwamura Y, Taoka M, Iriki A. Bilateral activity and callosal connections in the somatosensory cortex. Neuroscientist. 2001 Oct;7(5):419-29.

49. Taoka M, Toda T, Iriki A, Tanaka M, Iwamura Y. Bilateral receptive field neurons in the hindlimb region of the postcentral somatosensory cortex in awake macaque monkeys. Exp Brain Res. 2000 Sep;134(2):139-46.

50. Fabri M, Polonara G, Quattrini A, Salvolini U, Del Pesce M, Manzoni T. Role of the corpus callosum in the somatosensory activation of the ipsilateral cerebral cortex: an fMRI study of callosotomized patients. Eur J Neurosci. 1999 Nov;11(11):3983-94.

51. Fabri M, Polonara G, Quattrini A, Salvolini U. Mechanical noxious stimuli cause bilateral activation of parietal operculum in callosotomized subjects. Cereb Cortex. 2002 Apr;12(4):446-51.

52. Duquette M, Rainville P, Alary F, Lassonde M, Lepore F. Ipsilateral cortical representation of tactile and painful information in acallosal and callosotomized subjects. Neuropsychologia. 2008;46(8):2274-9.

53. Fabri M, Del Pesce M, Paggi A, Polonara G, Bartolini M, Salvolini U, et al. Contribution of posterior corpus callosum to the interhemispheric transfer of tactile information. Brain Res Cogn Brain Res. 2005 Jun;24(1):73-80.

54. Pandya DN, Karol EA, Heilbronn D. The topographical distribution of interhemispheric projections in the corpus callosum of the rhesus monkey. Brain Res. 1971 Sep 10;32(1):31-43.

55. Friston KJ, Harrison L, Penny W. Dynamic causal modelling. Neuroimage. 2003 Aug;19(4):1273-302.

56. Friston K. Dynamic causal modelling: <http://www.fil.ion.ucl.ac.uk/spm/>.

57. Stephan KE. On the role of general system theory for functional neuroimaging. J Anat. 2004 Dec;205(6):443-70.

58. Penny WD, Stephan KE, Mechelli A, Friston KJ. Comparing dynamic causal models. Neuroimage. 2004 Jul;22(3):1157-72.

59. Zhenghui Hu XZ, Huafeng Liu, and Pengcheng Shi. Nonlinear Analysis of the BOLD Signal. EURASIP Journal on Advances in Signal Processing 2009;2009:13.

60. Stephan KE, Weiskopf N, Drysdale PM, Robinson PA, Friston KJ. Comparing hemodynamic models with DCM. Neuroimage. 2007 Nov 15;38(3):387-401.

61. Lee L, Friston K, Horwitz B. Large-scale neural models and dynamic causal modelling. Neuroimage. 2006 May 1;30(4):1243-54.

62. Stephan KE, Marshall JC, Penny WD, Friston KJ, Fink GR. Interhemispheric integration of visual processing during task-driven lateralization. J Neurosci. 2007 Mar 28;27(13):3512-22.

63. Villemure C, Bushnell MC. Cognitive modulation of pain: how do attention and emotion influence pain processing? Pain. 2002 Feb;95(3):195-9.

64. Vuilleumier P, Richardson MP, Armony JL, Driver J, Dolan RJ. Distant influences of amygdala lesion on visual cortical activation during emotional face processing. Nat Neurosci. 2004 Nov;7(11):1271-8.

65. Pitt MA., Myung JI. When a good fit can be bad. Trends in Cognitive sciences. 2002 October; 6(10):421-425.

Annexe

Table A-1. Bayes Factors comparing Model 1 versus all the other 4-Region models, Level-3 condition. Comparison is for each subject (Subject 1-11), and across all subjects using the GBF and PER (Bayes Factors greater than 3 are highlighted) based on the conservative strategy proposed by Penny et al (58).

Model 1 Versus	Suje 1	Suje 2	Suje 3	Suje 4	Suje 5	Suje 6	Suje 7	Suje 8	Suje 9	Suje 10	Suje 11	Group Bays Factor	PER
Model 2	4.262	8.754	2.252	0.5019	3.05	7.525	3.833	2.344	0.2369	0.33	2.1	1.43E+03	5:2
Model 3	7.794	94.29	6.167	0.266		285.8	6.364	5.498		0.02847	15.14	5.20E+06	7:2
Model 4	19.5	20.26	19.47	16.26	14.2	20.16	20.32	20.15	3.908	18.19	20.5	2.14E+13	11:0
Model 5	73.48	326.4	85.16	1.22	15.89	148.9	44.3	52.41			44.54	6.10E+14	8:0
Model 6	156.5	1906	123.9		9.105	5818	127.6	113.1	1.724		3.03E+02	1.48E+19	8:0
Model 7	391.4	406.9	390.8	326.3	281.8	404.8	406.7	403.8	78.08	364.7	411.5	4.46E+27	11:0
Model 8	1459	6560	1708	24.28	267.4	2992	842.2	1050	12.49	5.532	893.7	1.73E+28	11:0
Model 9	1955	4.08E+04	2486	4.578	105.4	9.59E+04	1361	1468	30.03		5.68E+03	3.13E+30	10:0
Model 10	2188	3535	3009	780	1175	4129	1399	2465	10.52	2762	3704	3.27E+34	11:0
Model 11	5100	5.31E+04	5505	128.3	1121	2.05E+04	2898	4.50E+03	67.43	42.18	4896	7.98E+35	11:0
Model 12	1.11E+04	3.16E+05	1.77E+04	31.26	694	2.58E+05	7173	1.10E+04	221.3	4.906	2.78E+04	8.28E+38	11:0

Table A-2. ROI coordinates for each subject, Level-3 condition.

Subject #	S1L	S1R	S2L	S2R
Suje 1	-10, -48, 65	7, -45, 70	-58, -24, 20	62, -17, 25
Suje 2	-10, -45, 70	10, -41, 65	-62, -27, 25	62, -21, 25
Suje 3	-10, -48, 65	7, -41, 65	-65, -31, 20	58, -28, 25
Suje 4	-10, -41, 75	7, -48, 70	-55, -27, 20	55, -24, 25
Suje 5	-14, -45, 70	14, -45, 70	-62, -24, 20	62, -21, 20
Suje 6	-7, -48, 70	14, -45, 70	-65, -21, 15	65, -21, 25
Suje 7	-14, -38, 70	10, -45, 60	-52, -27, 20	62, -24, 20
Suje 8	-7, -38, 70	14, -38, 70	-65, -27, 20	65, -21, 25
Suje 9	-7, -48, 75	3, -48, 75	-55, -21, 20	62, -27, 20
Suje 10	-7, -41, 65	7, -45, 75	-62, -34, 25	62, -27, 30
Suje 11	-14, -38, 70	10, -38, 75	-62, -24, 25	62, -31, 25

Table A-3. ROI coordinates for each subject, Level-2 condition. Empty highlighted spaces indicate that no activation could be found in the GLM analysis which has been described in chapter 5.

Subject #	S1L	S1R	S2L	S2R
Suje 1	-3, -45, 60		-58, -24, 20	62, -21, 25
Suje 2	-10, -41, 70	7, -41, 70	-52, -21, 25	62, -17, 30
Suje 3	-10, -45, 70	7, -41, 70	-58, -21, 25	62, -27, 25
Suje 4	-10, -41, 75	3, -45, 70	-58, -27, 20	58, -21, 25
Suje 5	-7, -48, 65	14, -41, 70	-55, -27, 15	62, -21, 15
Suje 6	-7, -45, 70	10, -45, 75	-62, -21, 20	62, -24, 20
Suje 7	-3, -41, 60		-58, -21, 15	65, -24, 20
Suje 8	-10, -41, 75	10, -38, 75	-55, -27, 30	62, -21, 30
Suje 9	7, -48, 75	7, -48, 70	-58, -21, 20	58, -27, 20
Suje 10	-7, -45, 65	3, -45, 65	-52, -21, 20	65, -27, 30
Suje 11	-14, -34, 75	14, -34, 75	-58, -27, 20	58, -27, 20

Table A-4. ROI coordinates for each subject, Level-1 condition. Empty highlighted spaces indicate that no activation could be found in the GLM analysis which has been described in chapter 5.

Subject #	S1L	S2L	S2R
Suje 1	-7, -48, 65	-52, -24, 25	62, -21, 20
Suje 2	-10, -45, 65	-55, -24, 30	62, -21, 25
Suje 3	-7, -41, 65	-52, -27, 25	52, -24, 20
Suje 4	-14, -38, 75	-65, -27, 20	62, -21, 25
Suje 5	-10, -45, 70	-52, -21, 20	62, -27, 25
Suje 6	-7, -52, 70	-52, -31, 25	65, -27, 20
Suje 7			
Suje 8	-10, -41, 70	-52, -24, 35	62, -21, 25
Suje 9			
Suje 10	-10, -45, 65	-65, -27, 20	65, -27, 30
Suje 11	-7, -45, 65	-52, -21, 25	58, -24, 25